NETWORK SYNCHRONIZATION IN A NOISY ENVIRONMENT WITH TIME DELAYS

By

David Hunt

A Thesis Submitted to the Graduate

Faculty of Rensselaer Polytechnic Institute

in Partial Fulfillment of the

Requirements for the Degree of

DOCTOR OF PHILOSOPHY

Major Subject: PHYSICS

Approved by the
Examining Committee:

____
Dr. Gyorgy Korniss, Thesis Adviser

____
Dr. Boleslaw Szymanski, Thesis Adviser

____
Dr. Saraj Nayak, Member

____
Dr. Chjan Lim, Member

Rensselaer Polytechnic Institute
Troy, New York

December 2012
(For Graduation December 2012)

CONTENTS

LIST OF FIGURES

ABSTRACT

The ability of a network to synchronize can change drastically when time delays are introduced. Nonzero time delays impose a limitation on the strength/frequency of communication regarding the synchronizability of the network. When synchronization is possible, there is a fundamental limit on how well the network can synchronize, even in the most optimal circumstances. These fundamental properties are apparent even in the most basic case of uniform time delays in stochastic, linearly-coupled synchronization problems. This basic model can be expanded to include the richer behavior of networks with multiple delays. Non-uniform time delays can arise when there are multiple sources of delay, e.g. the time to transmit and the time to process information. In this particular two-delay case, the primary limitation on network synchronization does not come from restrictions in the transmission of a node's state to its neighbors; rather it depends on the ability for each node to process and respond to the information about itself in the context of its local environment. Furthermore, given a network's structure, there are optimal delays for which the network remains synchronizable for longer processing delays. As a result, synchronization is not always improved – and in some cases can be totally destroyed – by minimizing the transmission delays. For special cases, one can also study the scaling function that quantifies synchronization, showing the limitation of synchronization in a noisy network.

CHAPTER 1
Introduction [1]

Synchronization describes phenomena that involve a collection of agents coordinating among themselves to produce a global goal. The synchronization of a system emerges from the cumulative efforts of the individual entities, each regulating themselves based on what information they can gather of the system's overall state from neighbors. This information can be strongly distorted by noise, which prevents the achievement of perfect global consensus, and the focus becomes how controlled or wild the fluctuations tend to be about a steady state. A further obstacle to synchronization is the incompleteness of the data that each individual can act upon. There is no central director that guides the evolution of the system; rather each individual node within a network responds according to the information that it can gather from its immediate neighbors. (Although the goal is to understand such system that lack centralized governance, it will be insightful to consider fully connected systems, which exhibit some of the same critical behavior.) The final defining characteristic to be considered here is a time delay between the state of the system and an individual's reaction. The categorization of temporal delays can in general be split into two sources: from the transmission of state information between nodes and from the processing of that information or the execution of the response at a single node. The aim of this thesis is to explore and offer insight into the effects of noise and delays on the dynamics of various network topologies. To this end, in addition to the general theoretical results and numerical calculations, there will also be examples of different network topologies to show the relevant implications.

Crucial aspects of the underlying theory of delays have been long established in the context of macro-economic cycles as far back as 1935 [1, 2]. In such cases, describing the complex network reduces to a single stochastic variable [3, 4, 5]. The core feature that the inclusion of time delay presents in these models is os-

[1]Portions of this chapter to appear in: D. Hunt, G. Korniss, B.K. Szymanski, "Network Synchronization and Coordination in a Noisy Environment with Time Delays", (in review).

cillatory behavior, which under the appropriate conditions can be self-feeding and cause instability. The recent interest in the application of time delays to networks [6, 7, 8] offers fresh insights extending from these older results. Understanding the dynamics across a complex network offers the possibility to optimize synchronization [9, 10, 11, 12, 13]. The dynamics depend in part on the particular topology. Not only which nodes are connected to which is important, but strengths of each link can very, leading to weighted graphs [14, 15, 16]. All specific networks considered in this thesis are non-directional (two connected nodes communicate directly back and forth to each other), but there have been studies into directed graphs [6, 17, 18] and some general conclusions given here (e.g. in Section 3.9) can be applied to such cases. Two common topologies to be considered often in this thesis are the Barabási-Albert (BA) [19, 20] scale-free (SF) and the Erdős-Rényi (ER) random graphs [21]. To understand the difference between these network types, it is instructive to understand the artificial creation of such networks.

The degree distribution of BA networks is characterized by the exponential γ so that the probability that a randomly chosen node i has degree k_i follows $\mathrm{Prob}(k_i = x) \sim x^{-\gamma}$. The BA networks implemented throughout the numerical ensemble analyses fall within the $\gamma = 3$ family, set with a minimum degree of 3. The construction process of such networks involved creating a fully-connected core of nodes of this minimum degree. A new node is added by choosing 3 nodes within the existing core to which the new node is connected. This augmentation is repeated until the desired system size is reached, yielding a network with average degree $\langle k \rangle \approx 6$ (i.e. $\langle k \rangle \to 6$ as $N \to \infty$). Using this algorithm results in a correlated graph, in which higher degree nodes are likely to be connected to other higher degree nodes, and lower degree nodes are likely to be connected to lower degree nodes. One important feature to note is the existence of a central core of nodes of high degree.

The degree distribution of ER networks is binomial, which in the limit of large system size becomes Poisson [20, 21]. During the artificial construction, each possible link between nodes is considered and a true connection is realized with probability $\langle k \rangle/(N-1)$ (the factor of $N-1$ appears because self-links are disallowed). To be comparable with BA networks, the implemented ER networks have an average degree of 6. Because the algorithm does not ensure that the complete set of nodes constitutes a single connected component, any instance with multiple disjoint components is ignored, and a fresh trial is produced. Unlike BA networks, ER networks do not typically have a central core of nodes.

1.1 Example Applications

Studying synchronization has many applications to a diverse array of disciplines, as it can be used to described a variety of states that can interact in a network, e.g., pace, load, phase, or orientation. The following is a brief survey of topics to illustrate the general applicability as well as giving examples to enhance intuition (for alternative overviews, see [6, 9, 16, 22]).

Within a natural, ecological focus, time delays were introduced decades ago into population dynamics [23] and consequently elaborated upon, e.g. for systems with multiple predation levels [24]. A plethora of specific examples exist in ecology, from chirping cicadas and flashing fireflies [25] to herding and flocking of animals [26]. One specific instance of synchronization appears in bird flocks, where each bird adjusts its velocity to match the others, a crucial process in accomplishing such tasks as avoiding predators [27, 28]. Traders in the stock market benefit from synchronizing well with other traders as everyone seeks to balance the risk and reward in an uncertain environment [29]. Within a single organism, synchronization describes bursting neurons [30] and the propagation of excitatory fronts [31, 32, 33] in the brain. It also applies to postural sway [34, 35], and balancing a stick on one's finger [36, 37].

Shifting to artificial contexts, synchronization is important in controlling congestion in communication networks [6, 15, 16, 38, 39]. Delays from round trip times can lead to significant congestion on the internet [40]. Optimizing sychronization in important for managing virtual time horizons for massively parallel [41, 42] and distributed computing [43, 44]. Congestion control is of course also of interest in vehicular traffic [45, 46] and synchronization becomes crucial especially when autonomous vehicles are working cooperatively to stay in formation [47] or to carry out a task [39]. Technological applications utilize synchronization of coupled phase oscillators [48] as described by the well-studied Kuramoto model [49]) applies to flashing microfluidic arrays [50] and circuits comprised of optomechanical arrays [51].

1.2 The General Model

For each node i in a network, assign a local scalar state variable h_i. The two competing influences that continuously contribute to the evolution of each state variable are the noise η_i and the relaxational response to the node's local neighborhood. The response is linearly proportional to the difference between nodes i and j as defined by C_{ij}, where C is the coupling strength matrix. A local delay τ^{o} that comes from processing (cognitive) or execution, results in a lag in the information of the state of the node itself and its neighbor, while the transmission delay τ^{tr} only affects the information received from the neighbor. Hence each node obeys a delay differential equation of the form

$$\partial_t h_i(t) = -\sum_j C_{ij}[h_i(t-\tau_i^{\mathrm{o}}) - h_j(t-\tau_i^{\mathrm{o}}-\tau_{ij}^{\mathrm{tr}})] + \eta_i(t) \tag{1.1}$$

where the noise satisfies $\langle \eta_i(t)\eta_j(t')\rangle = 2D\delta_{ij}\delta(t-t')$, with D being the noise intensity. The system is initialized in a perfectly synchronized state ($h_i(t) \equiv 0$ for $t \leq 0$) with the noise becoming active at $t = 0$. Local delays are treated as an intrinsic property of each individual node, so every term in the sum includes the same delay (i.e. there is no j dependence). On the other hand, transmission delays may vary depending on the properties of the node at the other end of the link, so that every edge in the network can potentially have a unique delay. Setting $\eta_i(t) = 0$ for all i and t, Eq. (1.1) becomes deterministic and reduces to a the network consensus problem [6, 39]. In this context, the networked agents try to coordinate or reach an agreement or balance regarding a certain quantity of interest.

A standard measure of synchronization, coordination, or consensus in a noisy environment is the width [15, 41]

$$\langle w^2(t)\rangle = \left\langle \frac{1}{N}\sum_{i=1}^{N}[h_i(t) - \bar{h}(t)]^2 \right\rangle , \tag{1.2}$$

where $\bar{h}(t) = (1/N)\sum_{i=1}^{N} h_i(t)$ is the global average of the local state variables and $\langle \ldots \rangle$ denotes an ensemble average over the noise. A network is "synchronizable" if it asymptotically reaches a steady state with a finite width, i.e. $\langle w(\infty)\rangle < \infty$. When the network is well synchronized (or coordinated), the values h_i for all nodes are near the global mean $\bar{h}$ and the width is small.

1.3 Coordination without Time Delays

In order to distinguish the effects of noise from those coming from time delays, first consider the case of zero time delay. Explicitly, Eq. (1.1) takes the form

$$\partial_t h_i(t) = -\sum_j C_{ij}[h_i(t) - h_j(t)] + \eta_i(t) = -\sum_j \Gamma_{ij} h_j(t) + \eta_i(t) \tag{1.3}$$

where $\Gamma_{ij} = \delta_{ij}\sum_l C_{il} - C_{ij}$ is the network Laplacian. Writing the system of differential equations in relation to the network Laplacian is convenient, because it is the eigenvectors and eigenmodes of this matrix that will define the dynamics of the network. A special case of a Langevin equation, Eq. (1.3) describes an Edwards-Wilkinson process [52]. Starting from a flat initial profile ($h_i(0) = 0$ for all i) for symmetric couplings, the width evolves as [53]

$$\langle w^2(t)\rangle = \frac{D}{N}\sum_{k=1}^{N-1}\frac{(1 - e^{-2\lambda_k t})}{\lambda_k} , \tag{1.4}$$

where λ_k, $k = 0, 1, 2, \ldots, N-1$, are the eigenvalues of the network Laplacian. Note that measuring the local state variables h_i from the mean $\bar{h}$ in Eq. (1.2) removes the singular contribution of $\lambda_0 = 0$ (given that the network has a single connected component) associated with the uniform mode from the sum in Eq. (1.4). Consequently, the network is always synchronizable for *any* positive connection strengths with steady-state width

$$\langle w^2(\infty)\rangle = \frac{D}{N}\sum_{k=1}^{N-1}\frac{1}{\lambda_k}\ . \tag{1.5}$$

Clearly the larger contributions come from the modes with smaller eigenvalues.

In the limit of infinite network size, however, network ensembles with a vanishing Laplacian spectral gap may become unsynchronizable, depending on the details of the small-λ behavior of the density of eigenvalues [9, 15, 41]. This type of singularity is common in purely spatial networks (in particular, in low dimensions) where the relevant response functions and fluctuations diverge in the long-wavelength (small-λ) limit [41, 54]. In complex networks [19, 20, 55, 56] these singularities are typically suppressed as a result of sufficient amount of randomness in the connectivity pattern generating a gap or "pseudo" gap. [10, 41, 57, 58, 59, 60].

As is also clear from Eq. (1.5), synchronization can be arbitrarily improved in this case of no time delays, e.g., by uniformly increasing the coupling strength by a factor of $\sigma > 1$ (corresponding to more frequent communication). Such a re-weighting results in $C_{ij} \to \sigma C_{ij}$ ($\lambda_k \to \sigma\lambda_k$) and yields a width of

$$\langle w^2(\infty)\rangle_\sigma = \frac{1}{\sigma}\langle w^2(\infty)\rangle_{\sigma=1}\ . \tag{1.6}$$

The width is a monotonically decreasing function of σ; stronger effective coupling σ leads to better synchronization. A divergence in the width only comes about as the smallest eigenvalue vanishes, when the communication necessary to synchronize is overcome by noise.

CHAPTER 2
Uniform Local Time Delays [2]

Now that the effects of noise have been outlined in Section 1.3, let us turn our attention to those of nonzero time delays. Consider the case with symmetric coupling $C_{ij} = C_{ji}$ when transmission delays are negligible ($\tau_{ij}^{\mathrm{tr}} = 0$) and local delays are uniform ($\tau_i^o \equiv \tau$). Then Eq. (1.1) is governed by a single uniform time delay [61, 62]

$$\partial_t h_i(t) = -\sum_{j=1}^{N} C_{ij}[h_i(t-\tau) - h_j(t-\tau)] + \eta_i(t) = -\sum_{j=1}^{N} \Gamma_{ij} h_j(t-\tau) + \eta_i(t) \ . \quad (2.1)$$

This equation has a similar form to that of Eq. (1.3) but with the inclusion a delay τ. Since the delay is uniform, it is still possible to decompose the system into eigenmodes by diagonalizing the Laplacian.

2.1 Steady-state Fluctuations for a Single-Variable Stochastic Delay Equation

Before conducting the network analysis in this chapter and those following, it is useful to outline the general theory of a single variable with time delay and noise. It will be useful in understanding the underlying fluctuations of the system in the cases where the network Laplacian is diagonalizable. For generality, consider a single (linearized) stochastic variable $h(t)$ with multiple time delays $\{\tau_\omega\}_{\omega=1}^{\Omega}$ and noise, which obeys the linear first-order differential equation

$$\partial_t h(t) = A_0 h(t) + \sum_{\omega=1}^{\Omega} A_\omega h(t-\tau_\omega) + \eta(t) \ , \quad (2.2)$$

[2]Portions of this chapter to appear in: D. Hunt, G. Korniss, B.K. Szymanski, "Network Synchronization and Coordination in a Noisy Environment with Time Delays", (in review).

where $\langle \eta(t)\eta(t') \rangle = 2D\delta(t-t')$. A more suggestive form might be

$$\partial_t h(t) - A_0 h(t) - \sum_{\omega=1}^{\Omega} A_\omega h(t-\tau_\omega) = \eta(t-t') \; , \tag{2.3}$$

where the noise $\eta(t)$ plays the specific role of the inhomogeneous part. The corresponding Green's funtion $G(t,t')$ satisfies

$$\partial_t G(t,t') - A_0 G(t,t') - \sum_{\omega=1}^{\Omega} A_\omega G(t-\tau_\omega, t') = \delta(t-t') \; , \tag{2.4}$$

where the noise in Eq. (2.3) is replaced by $\delta(t-t')$. A Laplace transform performs the vital function of removing the heterogeneity of the arguments and turning them into multiplicative factors. The general transform is defined $\tilde{h}(s) = \int_0^\infty e^{-st} h(t) dt$, with the individual terms transforming as

$$\begin{aligned} \mathcal{L}[h(t)] &= \tilde{h}(s) \\ \mathcal{L}[\partial_t h(t)] &= s\tilde{h}(s) - h(t=0) = s\tilde{h}(s) \\ \mathcal{L}[h(t-\tau)] &= e^{-\tau s}\tilde{h}(s) \; , \\ \mathcal{L}[\delta(t-t')] &= e^{-st'} \end{aligned} \tag{2.5}$$

noting that $h(t) = 0$ for all $t < 0$. The transformed equation can then be written

$$s\tilde{G}(s) - A_0\tilde{G}(s) - \sum_{\omega=1}^{\Omega} A_\omega e^{-s\tau_\omega}\tilde{G}(s) = \left(s - A_0 - \sum_{\omega=1}^{\Omega} A_\omega e^{-s\tau_\omega} \right) \tilde{G}(s) = e^{-st'} \; . \tag{2.6}$$

The characteristic polynomial $g(s)$ associated with the homogeneous part of Eq. (2.6) is given by

$$g(s) \equiv s - A_0 - \sum_{\omega=1}^{\Omega} A_\omega e^{-\tau_\omega s} = 0 \; . \tag{2.7}$$

Efforts to determine the sycnhronizability of a system will reduce to finding the solutions of equations of this form.

Thus the Laplace transform of the Green's function of Eq. (2.2) has the form

$$\tilde{G}(s) = \frac{e^{-st'}}{g(s)} \; . \tag{2.8}$$

Performing the inverse transform, one finds

$$G(t,t') = \frac{1}{2\pi i}\int_{x_0-i\infty}^{x_0+i\infty} ds e^{st}\tilde{G}(s) = \frac{1}{2\pi i}\int_{x_0-i\infty}^{x_0+i\infty} ds \frac{e^{s(t-t')}}{g(s)} = \Theta(t-t')\sum_{\alpha}\frac{e^{s_\alpha(t-t')}}{g'(s_\alpha)} \; , \tag{2.9}$$

where s_α ($\alpha = 1, 2, \ldots$) are the (generally complex) zeros of the characteristic equation $g(s) = 0$ from Eq. (2.7). In the above inverse transform, the infinite line of integration is parallel to the imaginary axis ($s = x_0$) and is chosen to be to the right of all zeros of the characteristic polynomial. This allows for the application of the residue theorem (utilizing the quotient rule, which states that the residue of a function $f(z) = g(z)/h(z)$ about z_0 is $g(z_0)/h'(z_0)$) by closing the contour with an infinite semicircle to the left of this line. Note that the Green's function $G(t,t')$ depends only on the variable $t-t'$, reflecting the time translation symmetry of the problem.

Utilizing the Green's function, the general solution of Eq. (2.2) formally becomes

$$h(t) = \int_0^\infty dt' \; G(t,t')\eta(t') = \int_0^t dt' \; G(t,t')\eta(t') = \int_0^t dt' \; \sum_\alpha \frac{e^{s_\alpha(t-t')}}{g'(s_\alpha)} \, \eta(t') \; . \tag{2.10}$$

For more general initial conditions (other than uniformly zero for $t < 0$), see Ref. [63].

Averaging over the noise, the fluctuations of $h(t)$ become

$$\begin{aligned}
\langle h^2(t)\rangle &= \left\langle \int_0^t dt'\ \eta(t') \sum_\alpha \frac{e^{s_\alpha(t-t')}}{g'(s_\alpha)} \int_0^t dt''\ \eta(t'') \sum_\beta \frac{e^{s_\beta(t-t'')}}{g'(s_\beta)} \right\rangle \\
&= \int_0^t dt' \int_0^t dt''\ \sum_\alpha \frac{e^{s_\alpha(t-t')}}{g'(s_\alpha)} \sum_\beta \frac{e^{s_\beta(t-t'')}}{g'(s_\beta)} \langle \eta(t')\eta(t'')\rangle \\
&= \sum_{\alpha,\beta} \frac{1}{g'(s_\alpha)g'(s_\beta)} \int_0^t dt' \int_0^t dt''\ e^{s_\alpha(t-t')} e^{s_\beta(t-t'')} 2D\delta(t'-t'') \\
&= \sum_{\alpha,\beta} \frac{2D}{g'(s_\alpha)g'(s_\beta)} \int_0^t dt'\ e^{(s_\alpha+s_\beta)(t-t')} \\
&= \sum_{\alpha,\beta} \frac{-2D(1-e^{(s_\alpha+s_\beta)t})}{g'(s_\alpha)g'(s_\beta)(s_\alpha+s_\beta)}\ . \qquad (2.11)
\end{aligned}$$

The time dependence appears only in the terms $\exp((s_\alpha+s_\beta)t)$. Consequently, $h(t)$ reaches a stationary limit distribution for $t\to\infty$ of the form

$$\langle h^2(\infty)\rangle = \sum_{\alpha,\beta} \frac{-2D}{g'(s_\alpha)g'(s_\beta)(s_\alpha+s_\beta)}\ , \qquad (2.12)$$

with a finite variance when $\mathrm{Re}(s_\alpha) < 0$ for all α. When the steady state is reached, the zero with the largest real part of all s_α governs the long-time behavior of the stochastic variable $h(t)$. When the first zero requires a nonnegative real part, then $\langle h^2(t)\rangle$ diverges exponentially with time. Note that the condition for the existence of an asymptotic stationary limit distribution is the same as the one for the *stability* of the homogeneous part of Eq. (2.2) about the $h=0$ fixed point [39, 64]. Also keep in mind that Eq. (2.2) may have an arbitrary number of delays, so this analysis will still be applicable in future chapters when multiple delay sources are included.

2.2 Eigenmode Decomposition and Scaling

The first implementation of the Laplace transform analysis is to the present case of uniform time delays. By diagonalizing the symmetric network Laplacian Γ, the above set of equations of motion decouples into separate modes

$$\partial_t \tilde{h}_k(t) = -\lambda_k \tilde{h}_k(t-\tau) + \tilde{\eta}_k(t) \ , \tag{2.13}$$

where λ_k ($k = 0, 1, 2, \ldots, N-1$) are the eigenvalues of the network Laplacian, and $\tilde{h}_k$ and $\tilde{\eta}_k$ are the time-dependent components of the state and noise vectors, respectively, along the k-th eigenvector. Such an equation is known as an Ornstein-Uhlenbeck process [53]. Thus, the amplitude $\tilde{h}_k$ of each mode is governed by the same type of stochastic delay-differential equation

$$\partial_t \tilde{h}(t) = -\lambda \tilde{h}(t-\tau) + \tilde{\eta}(t) \ , \tag{2.14}$$

where the index k of the specific eigenmode is temporarily dropped for transparency and to streamline notation. The uniform mode with $\lambda_0 = 0$ is removed from the width, and only has contributions from noise, so one needs only to focus on the cases for which $\lambda > 0$.

The above stochastic delay-differential equation does has an exact stationary solution for the stationary-state variance [3, 5], but it can be insightful to first review the formal solution [61, 65]. Doing so can provide connections between the zeros of the underlying characteristic equation and the existence (and scaling) of the stationary-state fluctuations of the stochastic problem. The formal solution can also be applied to more general linear(-ized) problems with multiple time delays [66]. It also serves as the starting point from which one can extract the asymptotic behavior [67] near the singular points (synchronization boundary).

Performing standard Laplace transform on Eq. (2.14) in accordance with the method in Section 2.1, the characteristic equation associated with its homogeneous part is found to be

$$g(s) \equiv s + \lambda e^{-s\tau} = 0 \ . \tag{2.15}$$

The time-dependent fluctuations can be written formally as

$$\langle \tilde{h}^2(t) \rangle = \sum_{\alpha,\beta} \frac{-2D(1 - e^{(s_\alpha + s_\beta)t})}{g'(s_\alpha) g'(s_\beta)(s_\alpha + s_\beta)} \ . \tag{2.16}$$

The fluctuations remain *finite* (i.e., a stationary distribution exists) when

$$\mathrm{Re}(s_\alpha) < 0 \,, \tag{2.17}$$

for *all* α, where s_α, $\alpha = 1, 2, \ldots$, are the solutions of the characteristic equation, Eq. (2.15), on the complex plane. Inserting Eq. (2.15) into its derivative yeilds

$$g'(s) = 1 - \lambda\tau e^{-s\tau} = 1 + s\tau \,. \tag{2.18}$$

The expression for the fluctionations in Eq. (2.16) can then be simplified and becomes

$$\langle \tilde{h}^2(\infty)\rangle = \sum_{\alpha,\beta} \frac{-2D}{g'(s_\alpha)g'(s_\beta)(s_\alpha + s_\beta)} = \sum_{\alpha,\beta} \frac{-2D}{(1+\tau s_\alpha)(1+\tau s_\beta)(s_\alpha + s_\beta)} \,. \tag{2.19}$$

Eq. (2.15) is perhaps the oldest and most well-known transcendental characteristic equation from the theory of delay-differential equations [2, 39, 64, 68], with the linear stability analysis of numerous nonlinear systems reducing to this one. It has an infinite number of solutions for $\tau > 0$, but all have negative real parts for sufficiently small delay.

The condition for stability is easily derived in the case of uniform time delay by determining the point when the real part of a solution first vanishes. Begin with the real and imaginary parts of Eq. (2.15)

$$0 = \cos(s_I\tau) \tag{2.20}$$

$$-s_I = \sin(s_I\tau) \tag{2.21}$$

$$\tag{2.22}$$

where s_I is the imaginary part of s where the real part vanishes. Adding the squares of each equation gives $s_I = \pm\lambda$, which can then be inserted back into Eq. (2.20). Hence the condition in Eq. (2.17) holds if

$$\lambda\tau < \pi/2 \tag{2.23}$$

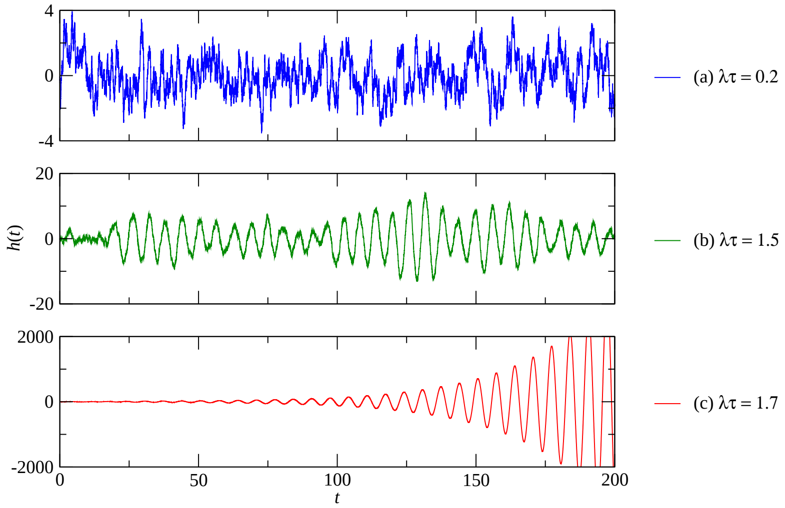

Figure 2.1: Time evolution of an individual mode obtained by numerically integrating Eq. (2.14) with $\lambda = 1$, $D = 1$, and $\Delta t = 0.001$ for several delays chosen to show the various behaviors across the separating/critical points $\lambda\tau = 1/e$ and $\pi/2$; (a) $\lambda\tau = 0.2 < 1/e$, (b) $1/e < \lambda\tau = 1.5 < \pi/2$, and (c) $\lambda\tau = 1.7 > \pi/2$.

since both λ and τ are strictly positive in the network topologies and circumstances of interest here.

Long-time dynamic behavior of the solution of Eq. (2.14) is governed by the zero(s) of Eq. (2.15) with the *greatest* real part. In particular, the zero with the largest real part is purely real for $\lambda\tau \leq 1/e$, hence no sustained oscillations occur, exemplified in Fig. 2.1(a). For $1/e < \lambda\tau < \pi/2$, all zeros including the ones with the largest real part have imaginary parts and are arranged symmetrically about the real axis. Thus the symmetry of the zeros is expected in the finding that the first zeros with vanishing real parts have imaginary parts of $\pm\lambda$. Nonzero imaginary parts result in persistent oscillations that do not diverge so long as condition (2.23) is satisfied, as shown in Fig. 2.1(b). The first pair of zeros to acquire positive real parts are the two with smallest imaginary parts. Once the product $\lambda\tau$ fails to satisfy the condition (2.23), the oscillation amplitude grows in time, as in Fig. 2.1(c). Specific time series for $\langle h^2(t) \rangle$ are shown in Fig. 2.2, where the real parts of solutions have become positive for delays $\tau = 1.60$ and 2.00 but remain negative for the others.

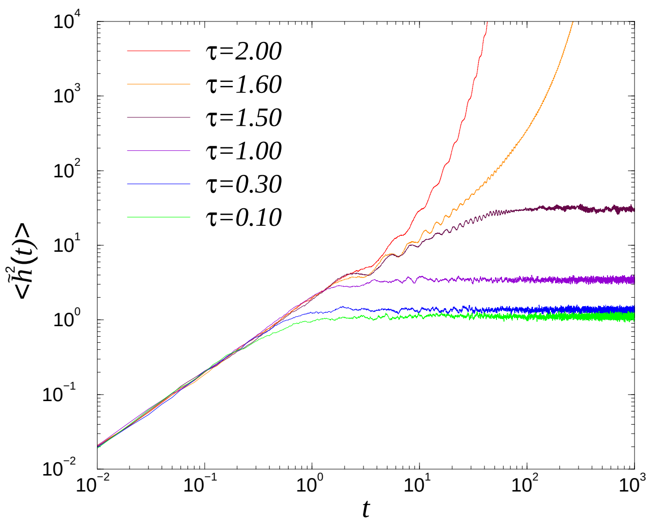

Figure 2.2: Time series of the fluctuations of a single mode ($\lambda = 1$) averaged over 10^4 realizations of noise (with $D = 1$) by numerically integrating Eq. (2.14) with $\Delta t = 0.01$ for different delays (from bottom to top in increasing order of τ).

2.3 Exact Scaling Functions for Time Delayed Stochastic Differential Equations

Küchler and Mensch [3] obtained the analytic stationary-state autocorrelation function for the stochastic delay-differential equation

$$\partial_t h(t) = ah(t) + bh(t - \tau) + \eta(t) \ , \tag{2.24}$$

with $\langle \eta(t)\eta(t')\rangle = 2D\delta(t - t')$.

An equation of this form appears in two cases that will be considered here. The first is the present focus of uniform time delays, with the special condition $a = 0$. The second case will come along in Chapter 3, when there will be two types of time delays. The specific application is viable for fully connected networks when there is transmission delay between nodes but no local delay. For this latter instance, it is useful to consider the full form of Eq. (2.24). The following derivation follows the steps in [3], but is set in the notation to match the present context of networks.

Define the stationary-state autocorrelation function as

$$K(t) = \langle h(t')h(t'+t)\rangle \ , \tag{2.25}$$

where it is implicitly assumed that $t' \to \infty$ to be applicable to the steady state. From this definition and the invariance under time translation in the stationary state, the autocorrelation function can be formally extended to $t < 0$ according to

$$K(t) = \langle h(t')h(t'+t)\rangle = \langle h(t'+t)h(t')\rangle = \langle h(t')h(t'-t)\rangle = K(-t) \ , \tag{2.26}$$

implying

$$\dot{K}(t) = -\dot{K}(-t) \ , \tag{2.27}$$

which will be needed later on.

As one would like to obtain a directly solvable equation of motion for the autocorrelation function, one must first find expressions for its time derivatives. Employing the equation of motion for $h(t)$ [Eq. (2.24)], one finds for $t \geq 0$ that

$$\begin{aligned}
\dot{K}(t) &= \partial_t K(t) = \partial_t \langle h(t')h(t'+t)\rangle = \langle h(t')\partial_t h(t'+t)\rangle \\
&= \langle h(t')\{ah(t'+t) + bh(t'+t-\tau) + \eta(t'+t)\}\rangle \\
&= a\langle h(t')h(t'+t)\rangle + b\langle h(t')h(t'+t-\tau)\rangle + \langle h(t')\eta(t'+t)\rangle \qquad (2.28) \\
&= aK(t) + bK(t-\tau) \ , \qquad (2.29)
\end{aligned}$$

using $\langle h(t')\eta(t'+t)\rangle = 0$ in the last step (i.e., Ito's convention [53, 69]). The above expression, combined with the (analytic) extension of the autocorrelation function in Eq. (2.26), yields the condition

$$\dot{K}(0) = aK(0) + bK(\tau) \tag{2.30}$$

in the limit of $t \to +0$. Differentiating Eq. (2.29) again with respect to t and exploiting the properties of Eqs. (2.26) and (2.27), the second derivative is found to be

$$
\begin{aligned}
\ddot{K}(t) &= a\dot{K}(t) + b\dot{K}(t-\tau) = a\dot{K}(t) - b\dot{K}(\tau - t) \\
&= a\{aK(t) + bK(t-\tau)\} - b\{aK(\tau - t) + bK(-t)\} \\
&= a\{aK(t) + bK(t-\tau)\} - b\{aK(t-\tau) + bK(t)\} \\
&= (a^2 - b^2)K(t) \ .
\end{aligned} \tag{2.31}
$$

Note that the reduction of the equation of motion of the autocorrelation function to a second order ordinary differential equation (with no delay) is a consequence of Eq. (2.24) having only one delay time-scale. The general solution of Eq. (2.31) can be written as

$$K(t) = A\cos(\omega t) + B\sin(\omega t) \tag{2.32}$$

with $\omega = \sqrt{b^2 - a^2}$. From the definition of the autocorrelation function in Eq. (2.25) and from some of the basic properties of the Green's function (see Section 2.3.1 for details), it also follows [3] that

$$\dot{K}(0) = \lim_{t\to 0} \partial_t \langle h(t')h(t'+t)\rangle = -D \ , \tag{2.33}$$

and from Eq. (2.30),

$$aK(0) + bK(\tau) = -D \ . \tag{2.34}$$

Thus, the second order ordinary differential equation Eq. (2.31) with conditions from Eqs. (2.33) and (2.34) can now be fully solved, yielding

$$A = K(0) = D\frac{-\omega + b\sin(\omega\tau)}{\omega[a + b\cos(\omega\tau)]} \ , \tag{2.35}$$

and

$$B = \frac{\dot{K}(0)}{\omega} = -\frac{D}{\omega} \ . \tag{2.36}$$

Finally, the stationary-state variance of the stochastic variable governed by Eq. (2.24) can be written as

$$\langle h^2(t)\rangle = \langle h(t)h(t)\rangle = K(0) = D\frac{-\omega + b\sin(\omega\tau)}{\omega[a+b\cos(\omega\tau)]} \ . \tag{2.37}$$

Following the technical detours and details in Section 2.3.1, Section 2.3.2 will cover the applications of the above result to obtain the scaling function of the fluctuations for the individual modes in specific networks.

2.3.1 General properties of the Autocorrelation Function and the Green's Function

From the definition of the autocorrelation function in Eq. (2.25) and of the Green's function in Eq. (2.10), it follows that

$$\begin{aligned} K(t) &= \langle h(t')h(t'+t)\rangle = \left\langle \int_0^{t'} du\ G(t',u)\eta(u) \int_0^{t'+t} dv\ G(t'+t,v)\eta(v) \right\rangle \\ &= \int_0^{t'} du \int_0^{t'+t} dv\ G(t',u)G(t'+t,v)\langle\eta(u)\eta(v)\rangle \\ &= 2D\int_0^{t'} du\ G(t',u)G(t'+t,u) \ , \end{aligned} \tag{2.38}$$

and consequently

$$\begin{aligned} \dot{K}(t) &= \partial_t\langle h(t')h(t'+t)\rangle = 2D\partial_t \int_0^{t'} du\ G(t',u)G(t'+t,u) \\ &= 2D\int_0^{t'} du\ G(t',u)\partial_t G(t'+t,u) \\ &= 2D\int_0^{t'} du\ G(t',u)(-\partial_u)G(t'+t,u) \\ &= -2D\int_0^{t'} du\ G(t',u)\partial_u G(t'+t,u) \ . \end{aligned} \tag{2.39}$$

Hence,

$$
\begin{aligned}
\dot{K}(0) &= -2D \lim_{t \to 0} \int_0^{t'} du\, G(t',u)\partial_u G(t'+t,u) \\
&= -2D \int_0^{t'} du\, G(t',u)\partial_u G(t',u) \\
&= -2D \int_0^{t'} du\, \partial_u \frac{G(t',u)^2}{2} \\
&= -D\{G(t',t') - G(t',0)\} = -D\{1-0\} = -D\ ,
\end{aligned}
\tag{2.40}
$$

where in the second term of the last expression $G(t',t') = 0$ and $G(t',0) \to 0$ as $t' \to \infty$. The former can be seen by a segment-by-segment integration and solution of Eq. (2.24) with a delta source $\delta(t-t')$ in the intervals $(t-t') \in [n\tau, (n+1)\tau]$, $n = 0, 1, 2, \ldots$ [3]; the solution in the $[0,\tau]$ interval is particularly simple, $G(t,t') = \exp[a(t-t')]$. The latter property is trivial in that the magnitude of the Green's function in the stationary state has to decay for large arguments.

2.3.2 Applications to Special Cases

2.3.2.1 Unweighted Symmetric Couplings with Uniform Local Delays

For symmetric couplings C_{ij} with uniform local delays, the Laplacian $\Gamma_{ij} = \delta_{ij}\sum_l C_{il} - C_{ij}$ in Eq. (2.1) can, in principle, be diagonalized. Each mode is governed by Eq. (2.13), a special case of Eq. (2.24) with $a = 0$, $b = -\lambda$, and $\omega = |b| = \lambda$ (λ being the eigenvalue of the respective mode). From Eq. (2.37), the steady-state variance of each mode then reduces to

$$
\langle h^2(\infty)\rangle = D\frac{1+\sin(\lambda\tau)}{\lambda\cos(\lambda\tau)} = D\tau\frac{1+\sin(\lambda\tau)}{\lambda\tau\cos(\lambda\tau)} = D\tau f(\lambda\tau)\ , \tag{2.41}
$$

yielding the analytic scaling function for each mode

$$
f(x) = \frac{1+\sin(x)}{x\cos(x)}\ , \tag{2.42}
$$

with the scaling variable $x = \lambda\tau$.

2.3.2.2 Complete Graphs with Only Uniform Transmission Delays

The exact stationary-state variance of Eq. (2.24) can also be applied to complete graphs with global coupling σ, which have no local delays but do have uniform transmission delays, i.e., Eq. (3.32) with $\gamma = 0$, translating to $a = -\sigma$, $b = -\sigma/(N-1)$ in Eq. (2.24). The analytic expression from Eq. (2.37) for the stationary-state variance for each (non-uniform) mode becomes

$$\langle h^2(\infty)\rangle = D\frac{\alpha + \frac{\sigma}{N-1}\sinh(\alpha\tau)}{\alpha[\sigma + \frac{\sigma}{N-1}\cosh(\alpha\tau)]} \ , \tag{2.43}$$

with $\alpha = \sqrt{a^2 - b^2} = \sigma\sqrt{1 - 1/(N-1)^2}$.

2.4 Scaling Function for Mode Fluctuations

To obtain the general scaling form of the fluctuations in the stationary state, define $z_\alpha \equiv \tau s_\alpha$ ($\alpha = 1, 2, \ldots$). One can easily see that the new variables z_α are the corresponding solutions of the scaled characteristic equation,

$$z + \lambda\tau e^{-z} = 0 \ , \tag{2.44}$$

and hence can *only* depend on $\lambda\tau$, i.e. $z_\alpha = z_\alpha(\lambda\tau)$. Thus,

$$s_\alpha(\lambda, \tau) = \frac{1}{\tau} z_\alpha(\lambda\tau) \ . \tag{2.45}$$

Substituting this into Eq. (2.19) yields

$$\langle \tilde{h}^2(\infty)\rangle = D\tau f(\lambda\tau) \ , \tag{2.46}$$

where

$$f(\lambda\tau) = \sum_{\alpha,\beta} \frac{-2}{(1+z_\alpha)(1+z_\beta)(z_\alpha + z_\beta)} \tag{2.47}$$

is the scaling function. Th scaling in Eq. (2.46) is illustrated by plotting $\langle \tilde{h}^2(\infty)\rangle/\tau$ vs $\lambda\tau$ as in Fig. 2.3, fully collapsing the data for different τ values (with fixed noise intensity D) .

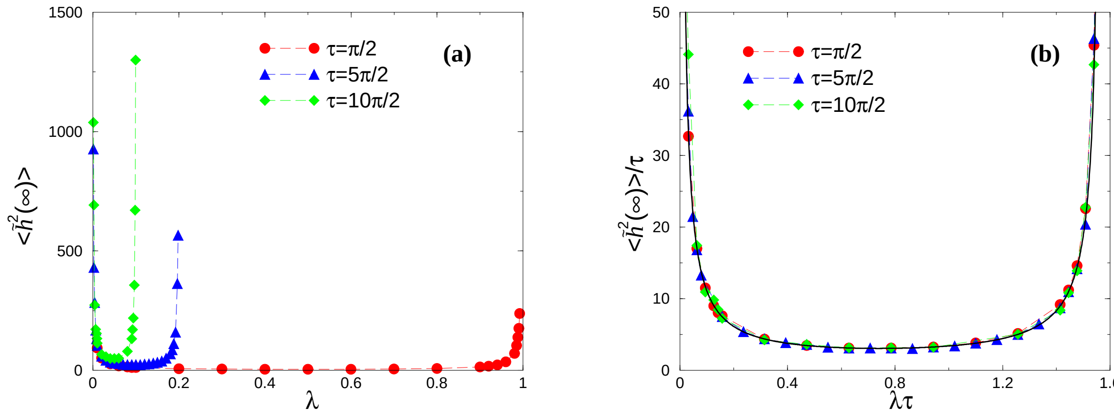

Figure 2.3: (a) Steady-state fluctuations of an individual mode as a function of λ obtained by numerical integration of Eq. (2.14) for several delays with $D = 1$ and $\Delta t = 0.01$. (b) Scaled fluctuations of an individual mode and the analytic scaling function Eq. (2.48).

As mentioned earlier, Eq. (2.14) has an exact solution for the stationary-state variance obtained by Küchler and Mensch [3] (briefly reviewed in Section 2.3), providing an exact form for the scaling function

$$f(\lambda\tau) = \frac{1+\sin(\lambda\tau)}{\lambda\tau\cos(\lambda\tau)} \, . \tag{2.48}$$

The asymptotic behavior of the scaling function near the singular points, $\lambda\tau = 0$ and $\lambda\tau = \pi/2$, can be immediately extracted from the exact solution given by Eq. (2.48) (see also Ref. [67] for a more generalizable method),

$$f(\lambda\tau) \simeq \begin{cases} \dfrac{1}{\lambda\tau} & 0 < \lambda\tau \ll 1 \\[2ex] \dfrac{4}{\pi(\pi/2-\lambda\tau)} & 0 < \dfrac{\pi}{2} - \lambda\tau \ll 1 \, . \end{cases} \tag{2.49}$$

The scaling function $f(x)$ $(x \equiv \lambda\tau)$ is clearly *non-monotonic*; it exhibits a single minimum, at approximately $x^* \approx 0.739$ with $f^* = f(x^*) \approx 3.06$, found through numerical minimization of Eq. (2.48). The immediate message of the above result is rather interesting: For a single stochastic variable governed by Eq. (2.14) with a nonzero delay, there is an optimal value of the "relaxation" coefficient, $\lambda^* = x^*/\tau$, at which point the stationary-state fluctuations attain their minimum value $\langle \tilde{h}^2(\infty)\rangle =$

$D\tau f^* \approx 3.06 D\tau$. This is in stark contrast with the zero-delay case (the standard Ornstein-Uhlenbeck process [53]) where $\langle \tilde{h}^2(\infty)\rangle = D/\lambda$, i.e., the stationary-state fluctuation is a monotonically decreasing function of the relaxation coefficient.

2.5 Implications for Coordination in Unweighted Networks

Since the eigenvectors of the Laplacian are orthogonal for symmetric couplings, the width can be expressed as the sum of the fluctuations for all non-uniform modes

$$\langle w^2(\infty)\rangle = \frac{1}{N}\sum_{k=1}^{N-1}\langle \tilde{h}_k^2(\infty)\rangle = \frac{D\tau}{N}\sum_{k=1}^{N-1} f(\lambda_k\tau) \ , \tag{2.50}$$

where λ_k is the eigenvalue of the kth mode. Thus, condition (2.23) must be satisfied for every $k > 0$ mode for synchronizability, or equivalently (as in the case of the deterministic consensus problem),

$$\lambda_{\max}\tau < \frac{\pi}{2} \ . \tag{2.51}$$

The above exact delay threshold for synchronizability has some profound consequences for unweighted networks. Here, the coupling matrix is identical to the adjacency matrix, $C_{ij} = A_{ij}$, and the bounds and the scaling properties of the extreme eigenvalues of the network Laplacian are well known. In particular [70, 71],

$$\frac{N}{N-1}k_{\max} \le \lambda_{\max} \le 2k_{\max} \ , \tag{2.52}$$

where $k_{\max}$ is the maximum node degree in the network [i.e., $\langle\lambda_{\max}\rangle = \mathcal{O}(\langle k_{\max}\rangle)$]. Thus, $\tau k_{\max} < \pi/4$ is sufficient for synchronizibility, while $\tau k_{\max} > \pi/2$ leads to the breakdown of synchronization with certainty. Note that this condition coincides with the convergence condition of the deterministic consensus problem [6, 39]. These inequalities imply that even a single (outlier) node with a sufficiently large degree can destroy synchronization or coordination in unweighted networks (regardless of the general trend, if any, of the tail of the degree distribution). Naturally, network realizations selected from an ensemble of random graphs with a power-law tailed degree distribution typically have large hubs, making them rather vulnerable

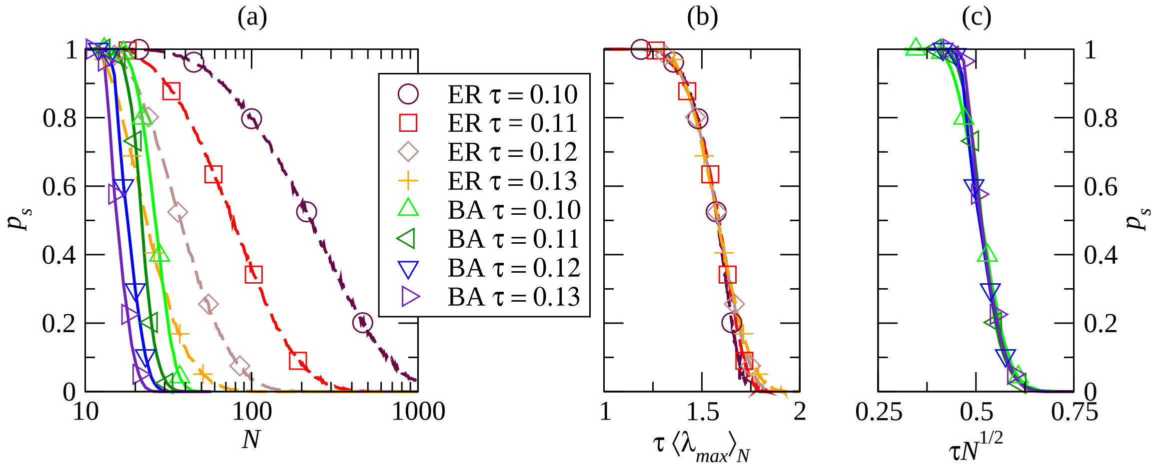

Figure 2.4: The fraction of synchronizable networks $p_s(\tau, N)$ taken from ensembles of 10^4 random constructions of ER and BA networks with $\langle k\rangle \approx 6$. (a) p_s vs. N. (b) and (c) are scaled plots of the same data according to Eq. (2.53), for ER and BA networks, respectively.

to intrinsic network delays [6, 39]. For example, Barabási-Albert (BA) [19, 20] and uncorrelated [72, 73] scale-free (SF) networks with structural degree cut-off (yielding $\lambda_{\max} \sim k_{\max} \sim N^{1/2}$) and similarly, SF network ensembles with natural cut-off (exhibting $\lambda_{\max} \sim k_{\max} \sim N^{1/(\gamma-1)}$) for $N \gg 1$ [56, 72]), are particularly vulnerable. Thus, for any fixed delay, increasing the size of scale free networks will eventually lead to the violation of condition (2.51), and in turn, to the breakdown of synchronization. In contrast, the typical largest degree (hence the largest eigenvalue of the Laplacian) grows much slower in ER random graphs [21], as $\lambda_{\max} \sim k_{\max} \sim \ln(N)$.

To illustrate the above finite-size dependence, define the fraction of synchronizable networks $p_s(\tau, N)$, which is equivalent to the probability that a randomly chosen realization of a network ensemble satisfies $\lambda_{\max} < \pi/2\tau$. Thus, $p_s(\tau, N) = P_N^<(\pi/2\tau)$, where $P_N^<(x)$ is the cumulative probability distribution of the largest eigenvalue of the network Laplacian. Figure 2.4 shows the fraction of synchronizable networks for BA and ER network ensembles by employing direct numerical diagonalization of the corresponding network Laplacians and evaluating condition (2.51) for each realization. For $N \gg 1$ the cumulative distribution for the largest eigenvalue exhibits the asymptotic scaling $P_N^{<}(x) \sim \phi(x/\langle\lambda_{\max}(N)\rangle)$ [60]. Thus, the fraction of synchronizable networks should scale as

$$p_{\rm s}(\tau, N) = P_N^{<}(\pi/2\tau) \sim \phi(\pi/2\tau\langle\lambda_{\max}(N)\rangle) = \psi(\tau\langle\lambda_{\max}(N)\rangle) \qquad (2.53)$$

Figure 2.4 (b) and (c) demonstrates the above scaling for ER and BA networks, respectively.

Since the scaling function is known exactly as Eq. (2.48), the eigenmode decomposition given by Eq. (2.50) allows one to evaluate the stationary width for an arbitrary network with a single uniform time delay by utilizing numerical diagonalization of the network Laplacian

$$\langle w^2(\infty)\rangle = \frac{D\tau}{N}\sum_{k=1}^{N-1} f(\lambda_k\tau) = \frac{D\tau}{N}\sum_{k=1}^{N-1}\frac{1+\sin(\lambda_k\tau)}{\lambda_k\tau\cos(\lambda_k\tau)}\ . \qquad (2.54)$$

The optimal (minimal) width occurs when all eigenvalues of the Laplacian are degenerate so that the couplings and/or delay can be tuned to the minimum of Eq. (2.48). For each mode in Eq. (2.54), such degeneracy is present in the case of a fully-connected network with uniform couplings, optimized to $C_{ij} = x^*/N\tau$ $(i \neq j)$ and $C_{ii} = 0$. For general networks, better synchronization can be achieved when the eigenvalue spectrum is narrow relative to the range of synchronizability so that most eigenvalues can fall near the minimum of Eq. (2.48). Strategies for achieving a narrow spectrum have been explored by others [17, 18], but are not a focus of this thesis.

2.6 Scaling, Optimization, and Trade-offs in Networks with Uniform Delays

With the knowledge of the scaling function in Eq. (2.54), one also immediately obtains the width for the case of an arbitrary but uniform effective coupling strength σ, where $C_{ij} = \sigma A_{ij}$. The effective coupling strength can now be tuned for optimal synchronization. However, there is a trade-off between how well the network synchronizes and the range over which it is synchronizable. When the eigenvalue spec-

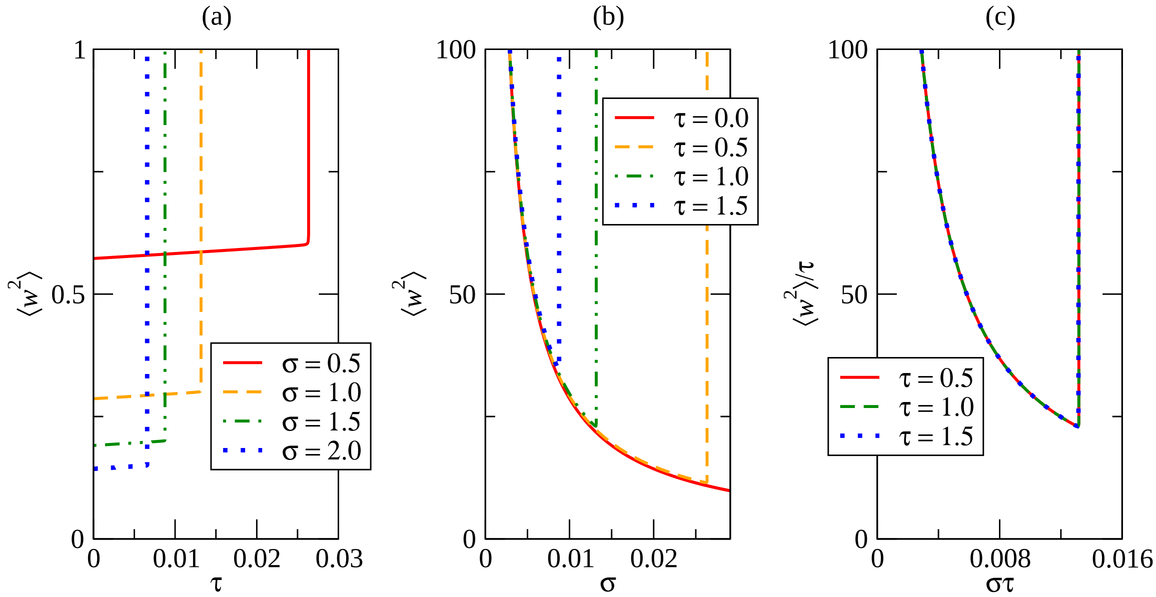

Figure 2.5: Stationary-state widths obtained through numerical diagonalization and utilizing Eq. (2.54) for a typical BA network with $N = 100$ (a) for several coupling strengths, (b) for several delays, and (c) scaled so that the nonzero delay curves collapse.

tum is not narrow, diminishing the couplings uniformly in order to satisfy Eq. (2.51) may cause small eigenvalues to be pushed farther up the left divergence of the scaling function. Figure 2.5(a) shows this trade-off in uniform reweighting ($C_{ij} \to \sigma C_{ij}$). The monotonicity of these widths means that the uniform delay should *always* be minimized to obtain the best synchronization. The same conclusion can be drawn from Fig. 2.5(b), which shows that networks synchronize better and do not become unsynchronizable until greater link strengths when the delay τ is minimized. Because globally reweighting the coupling strengths corresponds to a uniform scaling of the eigenvalues, define the width of a network by a scaling function $F(\sigma\tau)$ (see Fig. 2.5(c))

$$\langle w^2(\infty)\rangle_{\sigma,\tau} = \frac{D\tau}{N}\sum_{k=1}^{N-1} f(\sigma\lambda_k\tau) = D\tau F(\sigma\tau). \tag{2.55}$$

Fluctuations from small eigenvalues dominate other contributions to the width for small $\sigma\tau$, hence the optimal value occurs near the end of the synchronizable region, where the network fails to meet condition (2.51).

As an alternative to varying the (effective) uniform coupling strength σ, consider a scenario where the frequency (or rate) of communication is controlled for each node according to

$$\partial_t h_i(t) = -p_i(t) \sum_{j=1}^{N} A_{ij}[h_i(t-\tau) - h_j(t-\tau)] + \eta_i(t) \; . \qquad (2.56)$$

In the above scheme, $p_i(t)$ is a binary stochastic variable for each node, such that at each discretized time step, $p_i(t) = 1$ with probability p and $p_i(t) = 0$ with probability $1-p$ (for simplicity, consider uniform communication rates). The local network neighborhood remains fixed, while nodes communicate with their neighbors only at rate p at each time step. As an application for trade-off, consider a system governed by the above equations and stressed by large delays, where local pairwise communications at rate p=1 would yield unsynchronizability, i.e., $\tau\lambda_{\max} > \pi/2$ (see Fig. 2.6). The width diverges for one of two reasons: either communication is too frequent and the system fails to satisfy condition (2.51), or there is no synchronization (p=0) and the system is overcome by noise. However, the divergence of the width is faster in the former, accelerated by overcorrections made by each node due to the delay. With an appropriate reduction in the communication rate, the width reaches a finite steady state, recovering synchronizability, as can be seen in Fig. 2.6. Decreasing the frequency of communication can counter-intuitively allow a network to become synchronizable for delays and couplings that would otherwise cause the width to diverge.

2.7 Coordination and Scaling in Weighted Networks

For the case of uniform delays, compare the following two cases: networks with weights that have been normalized locally by node degree and networks with weights that are globally uniform. The couplings for local weighting are defined as $C_{ij} = \sigma A_{ij}/k_i$ (a common weighting scheme in generalized synchronization problems [9]), while for uniform couplings $C_{ij} = \sigma A_{ij}/\langle k\rangle$. In turn, the weighted (or normalized) Laplacian becomes $\Gamma = \sigma K^{-1}L$ where K is the diagonal matrix with node degrees

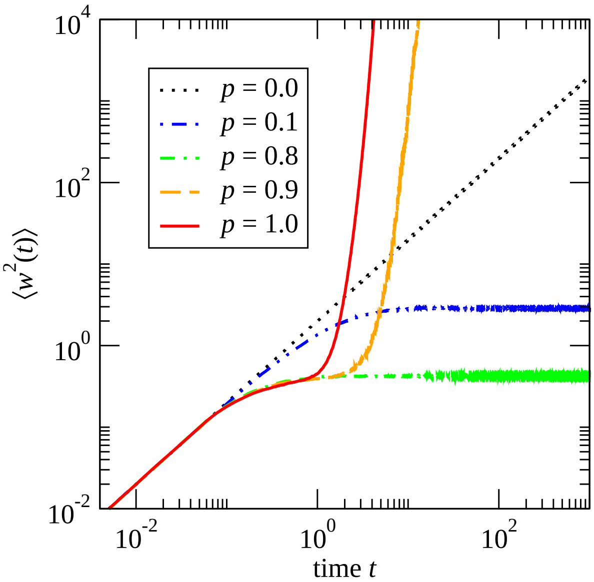

Figure 2.6: Time evolution of the width obtained by numerically integrating Eq. (2.56) with D=1, Δt=0.005, and averaged over 10^3 realizations of noise for several communication rates p on a BA network of size N=100 and average degree $\langle k \rangle$=6 with $\tau\lambda_{\max} = 1.2 \times \pi/2$.

on its diagonal, $K_{ij} = \delta_{ij} k_i$, and L is the graph Laplacian, $L_{ij} \equiv \delta_{ij} \sum_l A_{il} - A_{ij} = \delta_{ij} k_i - A_{ij}$. Similarly, for uniform couplings, the corresponding Laplacian becomes $\Gamma = \sigma \langle k \rangle^{-1} L$. Note that the overall coupling strength (communication cost) is the same in both cases, $\sigma \sum_{ij} A_{ij}/k_i = \sigma \sum_{ij} A_{ij}/\langle k \rangle = \sigma N$.

In the locally-weighted case, the eigenvalue spectrum of $K^{-1}L$ is known to be confined within the interval $[0, 2]$ [74], so any network of this class will be synchronizable, provided $\sigma\tau < \pi/4$. With globally uniform weighting, the increase of $\lambda_{\max}$ with N will lead to fewer synchronizable networks as N grows (holding $\langle k \rangle$ constant). Figure 2.7(a) shows that it is more likely for an ER network to be synchronizable than a BA network of the same size N when the couplings are weighted uniformly by $\langle k \rangle$ (with all ER networks remaining synchronizable over the range of N for the two smallest delays). However, this is not always the case when couplings are weighted locally by node degree (Fig. 2.7(b)), although nearly all of these networks remain synchronizable over the delays in Fig. 2.7(a). The behavior of the width for typical

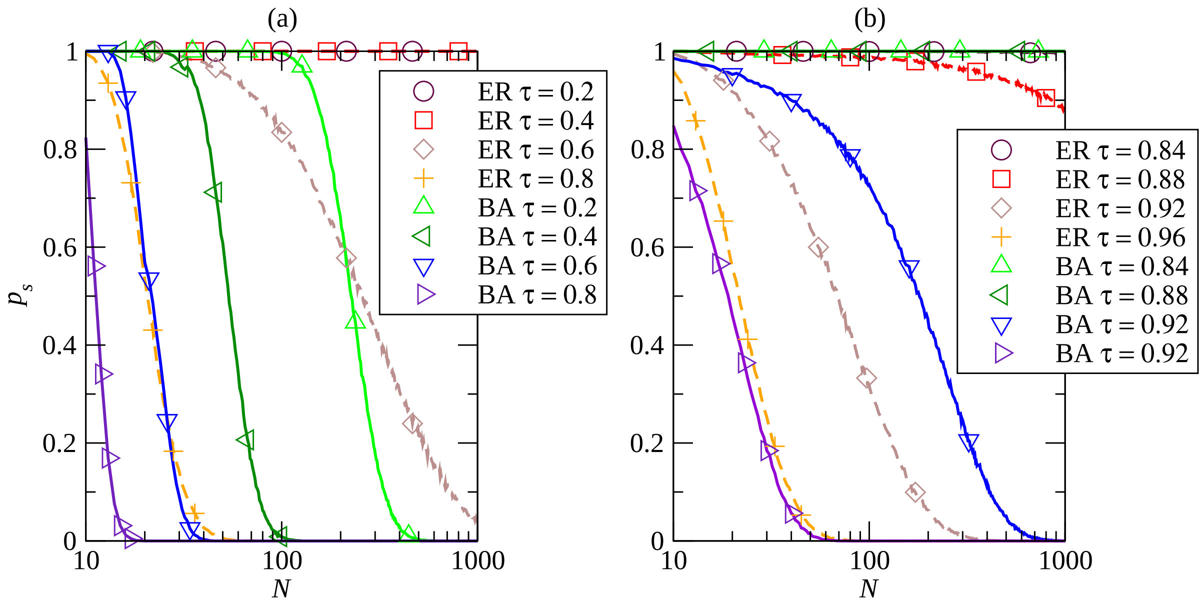

Figure 2.7: Fraction of synchronizable networks for (a) uniform global weights and (b) local weights for the same ensemble of networks used in Fig. 2.4.

networks is shown in Fig. 2.8 to compare the effects of these two normalizations. In both the BA and ER case, synchronization is better and is maintained for longer delays when the coupling strengths are weighted locally by node degree.

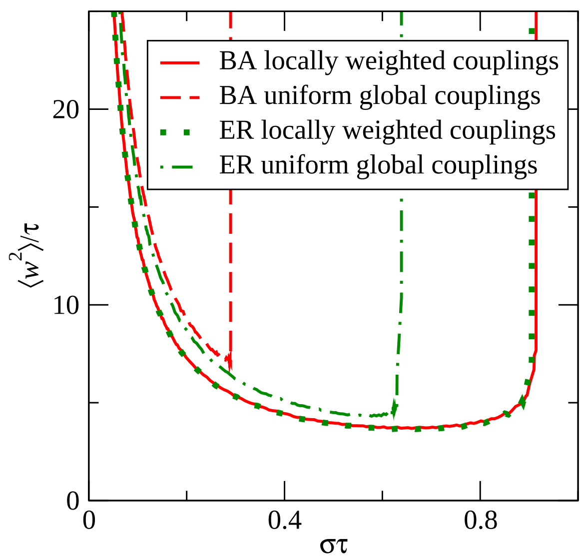

Figure 2.8: Scaled widths simulated with $\Delta t = 0.01$ of a typical BA and a typical ER network, each of size $N = 100$ and with $\langle k \rangle = 6$.

CHAPTER 3
Multiple Time Delays [3]

To generalize the basic model, let us distinguish between transmission and processing time delays. With the introduction of transmission delay, the information that a node has about its local neighborhood is not as recent as the information that is has on itself. The response of a node depends on its state within the context of an even older snapshot of its neighbors. As a starting point, consider the case when this transmission delay is uniform, so that Eq. (1.1) becomes

$$\partial_t h_i(t) = -\sum_j C_{ij}[h_i(t-\tau_{\mathrm{o}}) - h_j(t-\tau_{\mathrm{o}}-\tau_{\mathrm{tr}})] + \eta_i(t) \tag{3.1}$$

where the local delay τ_{o} and the transmission delay τ_{tr} are the same for all nodes and links, respectively. Although the synchronizability condition and steady state width cannot be determined in a closed form for arbitrary networks as is the case of Eq. (2.1), focusing on special cases does offer insight.

3.1 A Stochastic Model of Two Coupled Nodes with Local and Transmission Delays

The absolutely simplest case consists of two coupled nodes. Although the idea of a network is lost for $N = 2$, there still exists nontrivial critical behavior and the simplification, as will be shown, permits an analysis of the asymptotic behavior of the width. With only two nodes, the system of two coupled delay differential

[3] Portions of this chapter previously appeared as: D. Hunt, G. Korniss, B.K. Szymanski, "The impact of competing time delays in coupled stochastic systems", Phys. Lett. A **375**, 880 (2011). Other portions of this chapter to appear in: D. Hunt, G. Korniss, B.K. Szymanski, "Network Synchronization and Coordination in a Noisy Environment with Time Delays", (in review).

equations becomes

$$\begin{aligned} \partial_t h_1(t) &= -\lambda[h_1(t-\tau_{\rm o}) - h_2(t-\tau_{\rm o}-\tau_{\rm tr})] + \eta_1(t) \\ \partial_t h_2(t) &= -\lambda[h_2(t-\tau_{\rm o}) - h_1(t-\tau_{\rm o}-\tau_{\rm tr})] + \eta_2(t) \end{aligned} \tag{3.2}$$

where $\lambda > 0$ is the coupling strength between the two nodes.

To simplify notation, let $\gamma \equiv \tau_{\rm o}/(\tau_{\rm o}+\tau_{\rm tr}) = \tau_{\rm o}/\tau$ ($0 \le \gamma \le 1$). Further, focus on the relative difference $u(t) = h_2(t) - h_1(t)$, which is related to the width as $\langle u^2 \rangle = \langle (2w)^2 \rangle$. The quantity $u(t)$ is governed by the equation

$$\partial_t u(t) = -\lambda u(t-\gamma\tau) - \lambda u(t-\tau) + \xi(t)\ , \tag{3.3}$$

where $\langle \xi \rangle = 0$ and $\langle \xi(t)\xi(t') \rangle = 4D\delta(t-t')$. The special case $\gamma = 1$ of the above equation reduces directly to the case of uniform delay in Chapter 2. The quantity of interest is $\langle u^2(t) \rangle$, capturing the relative deviation of the relevant state variables on the two nodes. By definition, the system is synchronizable if the fluctuations reach a finite steady state, $\langle u^2(\infty) \rangle < \infty$. In the absence of time delays (τ=0) one immediately finds $\langle u^2(t) \rangle = (D/\lambda)(1-e^{-4\lambda t})$ [53], i.e., the system is synchronizable for any $\lambda > 0$. Further, the stronger the coupling, the better the synchronization: $\langle u^2(\infty) \rangle = D/\lambda$ is a monotonically decreasing function of λ.

Employing standard Laplace transform [61, 63], one can immediately write the formal solution for Eq. (3.3)

$$u(t) = \int_0^t dt' \xi(t') \sum_\alpha \frac{e^{s_\alpha (t-t')}}{h'(s_\alpha)}\ , \tag{3.4}$$

where s_α, $\alpha = 1, 2, \ldots$, are the zeros of the characteristic equation

$$g(s) \equiv s + \lambda e^{-\gamma\tau s} + \lambda e^{-\tau s} = 0 \tag{3.5}$$

on the complex plane. Then for the noise-averaged fluctuations one finds

$$\begin{aligned}\langle u^2(t)\rangle &= \sum_{\alpha,\beta} \frac{-4D(1-e^{(s_\alpha+s_\beta)t})}{g'(s_\alpha)g'(s_\beta)(s_\alpha+s_\beta)} \\ &= \sum_{\alpha,\beta} \frac{-4D(1-e^{(s_\alpha+s_\beta)t})}{(1-\gamma\lambda\tau e^{-\gamma\tau s_\alpha}-\lambda\tau e^{-\tau s_\alpha})(1-\gamma\lambda\tau e^{-\gamma\tau s_\beta}-\lambda\tau e^{-\tau s_\beta})(s_\alpha+s_\beta)} \\ &= \sum_{\alpha,\beta} \frac{-4D\tau(1-e^{(z_\alpha+z_\beta)t/\tau})}{(1-\gamma\lambda\tau e^{-\gamma z_\alpha}-\lambda\tau e^{-z_\alpha})(1-\gamma\lambda\tau e^{-\gamma z_\beta}-\lambda\tau e^{-z_\beta})(z_\alpha+z_\beta)}\ , \qquad (3.6)\end{aligned}$$

where the last expression of the above equation introduces the scaled variables $z_\alpha \equiv \tau s_\alpha$. From Eq. (3.5) and from the definition of these scaled variables it is evident that z_α are the solutions of the scaled characteristic equation

$$z + \lambda\tau e^{-\gamma z} + \lambda\tau e^{z} = 0\ , \qquad (3.7)$$

and consequently, the solutions depend only on $\lambda\tau$, i.e., $z_\alpha = z_\alpha(\lambda\tau)$. From the structure of the above characteristic equation it follows that if z is a solution of Eq. (3.7) so is its complex conjugate z^*. From Eq. (3.6) it is clear that synchronization can only be achieved if $\mathrm{Re}(z_\alpha)<0$ for *all* α. To identify the boundary of the region of synchronizability, one has to find the solution(s) with a vanishing real part, i.e., $z = x+iy$ with $x = 0$ [2, 24, 64, 68]. Elementary analysis yields $y_c^{\pm}=\pm\pi/(1+\gamma)$ and

$$(\lambda\tau)_c = \frac{\pi}{2(1+\gamma)} \sec\left(\frac{\pi}{2}\frac{1-\gamma}{1+\gamma}\right)\ . \qquad (3.8)$$

Thus, for a fixed γ, the system is synchronizable if $0 < \lambda\tau < (\lambda\tau)_c(\gamma)$. Results obtained by numerically integrating Eq. (3.3) together with the analytic expression Eq. (3.8) are shown in Fig. 3.1. The time discretization of Eq. (3.3) naturally has its own effects on the stability through the numerical scheme. Choosing $\Delta t \ll \gamma\tau$ and $\Delta t \ll 1/\lambda$ will yield only small corrections to the behavior of the underlying continuous-time system. The phase diagram and some limiting cases will be discussed in terms of the original variables, the local delay τ_o and the transmission delay τ_{tr}, in section 3.4.

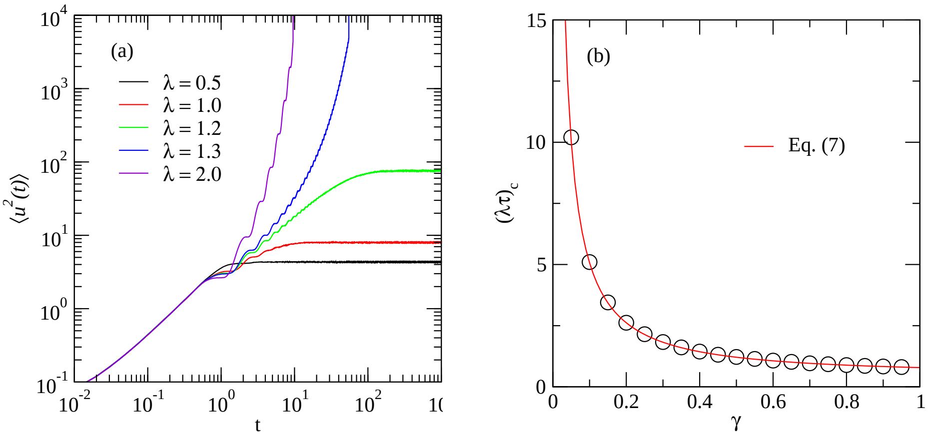

Figure 3.1: (a) Time series $\langle u^2(t)\rangle$ for τ=1.00, γ=0.50 for different values of the coupling constant λ. Here, and throughout this paper, D=1 and Δt=0.01. (b) Synchronizability threshold in terms of the scaled variable $\lambda\tau$ vs γ. Data points were obtained by numerically integrating Eq. (3.3) . The solid line represents the exact analytic expression Eq. (3.8).

3.2 Scaling and Asymptotics in the Steady State

The next step is to analyze the steady-state fluctuations, in particular, their scaling behavior in the synchronizable regime, $0 < \lambda\tau < (\lambda\tau)_c(\gamma)$. Here, the fluctuations remain finite, and in the steady state ($t \to \infty$) from Eq. (3.6) one obtains

$$\langle u^2(\infty)\rangle = D\tau f(\gamma, \lambda\tau) \; , \tag{3.9}$$

where

$$f(\gamma,\lambda\tau) = \sum_{\alpha,\beta} \frac{-4}{(1-\gamma\lambda\tau e^{-\gamma z_\alpha} - \lambda\tau e^{-z_\alpha})(1-\gamma\lambda\tau e^{-\gamma z_\beta} - \lambda\tau e^{-z_\beta})(z_\alpha + z_\beta)} \tag{3.10}$$

is the scaling function for the steady-state fluctuations. [Recall that $z_\alpha = z_\alpha(\lambda\tau)$ are the solutions of the scaled characteristic equation Eq. (3.7).] Thus for a given γ,

$$\frac{\langle u^2(\infty)\rangle}{D\tau} = f(\lambda\tau) \; , \tag{3.11}$$

where in this notation, the γ-dependence is supressed to highlight the scaling behavior of the fluctuations, which is valid for each γ separately. Figure 3.2 shows

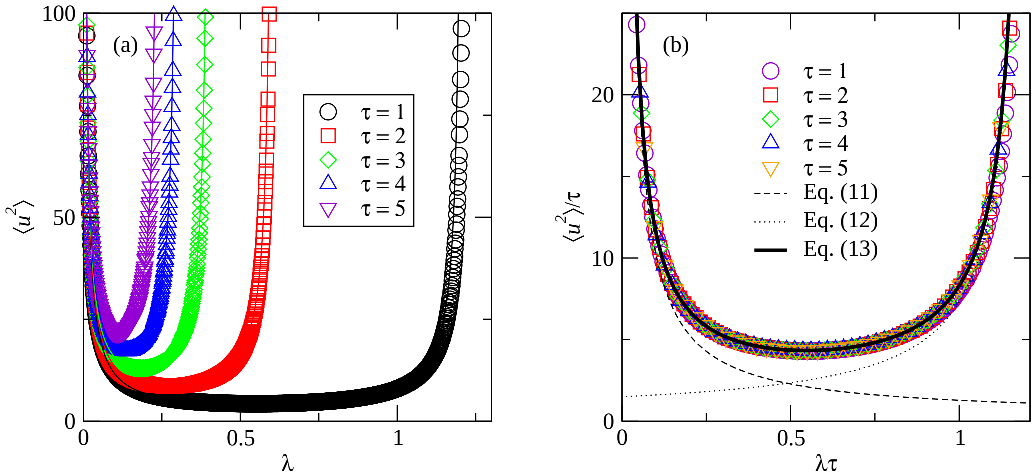

Figure 3.2: (a) Steady-state fluctuations as a function of the coupling strength λ for the various delays for γ=0.5. Data points are obtained by numerically integrating Eq. (3.3). (b) Same data as in (a) scaled according to Eq. (3.11), $\langle u^2(\infty)\rangle/\tau$ vs $\lambda\tau$. The dashed lines represent the asymptotic behaviors of the scaling function near the two endpoints of the synchronizable regime , Eqs. (3.12) and (3.13), respectively, while the solid line (running precisely through the data points) represents the full approximate scaling function $f(\lambda\tau)$, Eq. (3.14).

the steady-state fluctuations before (a) and after (b) scaling, and demonstrates the data collapse for the scaled variables according to Eq. (3.11). The scaling function $f(\lambda\tau)$ (shown in Fig. 3.2(b)) is a non-monotonic function of its argument, diverging at $\lambda\tau = 0$ and $\lambda\tau = (\lambda\tau)_c(\gamma)$, and exhibiting a single minimum between these points. This non-monotonic feature of the scaling function with a single minimum between $0 < \lambda\tau < (\lambda\tau)_c(\gamma)$ is present for all $0 < \gamma \leq 1$. Figure 3.3 shows several of these curves for various ratios of the delay γ. Thus, for fixed non-vanishing and finite delays, there is an optimal value of the coupling constant λ for which the steady-state fluctuation attains its minimum value. For stronger couplings, the overall coordination between the two nodes weakens, and for $\lambda > (\lambda\tau)_c(\gamma)/\tau$, it completely deteriorates.

The fluctuations of $\langle u^2(\infty)\rangle$ diverge at the end points of the synchronizable regime [as at least for one α, $\text{Re}(z_\alpha) \to 0$], indicating the breakdown of synchro-

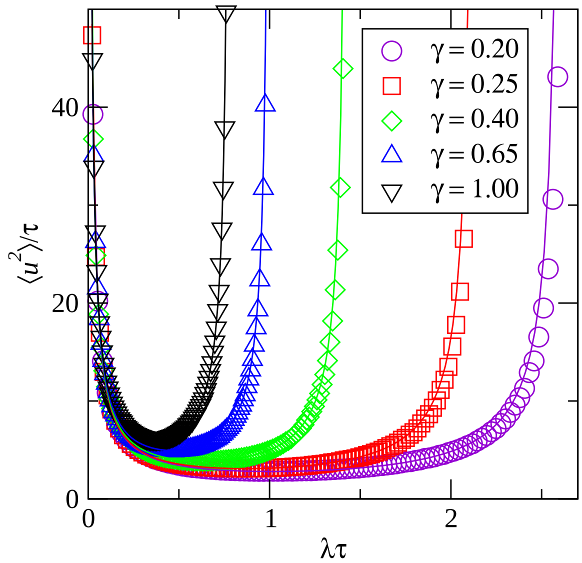

Figure 3.3: Scaled steady-state fluctuations $\langle u^2(\infty)\rangle/\tau$ vs $\lambda\tau$ for various γ values. Data points are obtained by numerically integrating Eq. (3.3). Solid lines represent the full approximate scaling function $f(\lambda\tau)$ for each γ, Eq. (3.14).

nization. Near these endpoints, the sum in Eq. (3.10) is dominated by the term(s) where $\mathrm{Re}(z_\alpha) \simeq 0$ [67]. These are the solutions which have (negative) real parts with the smallest amplitude. To leading order,

$$f(\lambda\tau) \simeq \frac{1}{\lambda\tau} \tag{3.12}$$

as $\lambda\tau \to 0$, and

$$f(\lambda\tau) \simeq \frac{c_1(\gamma)}{(\lambda\tau)_c(\gamma) - \lambda\tau} \tag{3.13}$$

as $\lambda\tau \to (\lambda\tau)_c$ ($\lambda\tau \lesssim (\lambda\tau)_c$) with $c_1(\gamma)$ given in Section 3.3 by Eq. (3.22). From the numerical results shown in Fig. 3.2(b), it is also apparent that the scaling function varies slowly between (and away from) the singular points. Thus, $f(\lambda\tau)$ can be reasonably well approximated [67] throughout the full synchronizable regime $0 < \lambda\tau < (\lambda\tau)_c(\gamma)$ by

$$f(\lambda\tau) \approx \frac{1}{\lambda\tau} + \frac{c_1(\gamma)}{(\lambda\tau)_c(\gamma) - \lambda\tau} + c_2(\gamma), \tag{3.14}$$

with $c_2(\gamma)$ also given in Section 3.3 by Eq. (3.26).

Figure 3.2(b) and Fig. 3.3 show that the above approximate scaling function Eq. (3.14) (being asymptotically exact near the singular points) matches the numerical data very well. In particular, it captures the basic non-monotonic feature of the results obtained from numerical integration, exhibiting a single minimum

$$(\lambda\tau)_{\min}(\gamma) = \frac{(\lambda\tau)_{\mathrm{c}}(\gamma)}{1+\sqrt{c_1(\gamma)}} \tag{3.15}$$

in the $0 < \lambda\tau < (\lambda\tau)_{\mathrm{c}}(\gamma)$ interval. Since the above analytic estimate for $(\lambda\tau)_{\min}(\gamma)$ is based on asymptotics, it is worthwhile to compare it to the actual numerical estimates. From the data and for the γ values shown in Fig. 3.3, the relative deviation between the estimate and Eq. (3.15) is 0.7%, 0.7%, 0.7%, 0.5%, and 0.4% for $\gamma = 0.20, 0.25, 0.40, 0.65$, and 1.00, respectively.

As can also be seen in Fig. 3.3, the theoretical asymptotic behavior, captured by the approximate scaling function Eq. (3.14) becomes less accurate for small γ near $(\lambda\tau)_{\mathrm{c}}(\gamma)$. Other than lacking higher-order corrections to the asymptotic expressions, this is due in part to the time discretization in the numerical integration. For sufficiently small γ values, the condition $\Delta t << \gamma\tau$ will not hold, and deviations between the results of the time-discretized numerical scheme and those of the continuous system Eq. (3.3) will become more significant and noticeable.

3.3 Asymptotic Behavior of the Scaling Function Near the Synchronization Thresholds

Applying the method in Ref. [67] (which was used to analyze the scaling function for uniform delays) to the present case gives the dominant contributions in Eq. (3.10) nea the boundaries of the synchronizable regime. First, assume that solutions of the characteristic equation

$$z + \lambda\tau e^{-\gamma z} + \lambda\tau e^{-z} = 0 \tag{3.16}$$

change continuously with the product $\lambda\tau$. Thus, if z=z_o is a solution for $\lambda\tau = (\lambda\tau)_o$, then for a small change in the parameter, $\lambda\tau = (\lambda\tau)_o + \delta\lambda\tau$, the corresponding solution can be written as $z = z_o + \delta z$. Substituting this into the characteristic equation, to lowest order this becomes

$$\delta z \simeq -\frac{e^{-\gamma z_o} + e^{-z_o}}{1 - \gamma(\lambda\tau)_o e^{-\gamma z_o} - (\lambda\tau)_o e^{-z_o}} \delta\lambda\tau + \mathcal{O}\left((\delta\lambda\tau)^2\right) \ . \tag{3.17}$$

For $\lambda\tau = 0$, there is a single solution with vanishing real part, z=0, thus for small $\lambda\tau$

$$z(\lambda\tau) \simeq -2\lambda\tau + \mathcal{O}((\lambda\tau)^2) \ . \tag{3.18}$$

The dominant contribution for the scaling function as $\lambda\tau \rightarrow 0$ comes from the corresponding term in Eq. (3.10), to leading order yielding

$$f(\lambda\tau) \simeq \frac{-4}{2(-2\lambda\tau)} = \frac{1}{\lambda\tau} \ . \tag{3.19}$$

For $\lambda\tau = (\lambda\tau)_\mathrm{c}(\gamma)$ [Eq. (3.8)], there is a pair of solutions (complex conjugates) with vanishing real parts $z = \pm i\frac{\pi}{1+\gamma}$. When $\lambda\tau$ is in the vicinity of $(\lambda\tau)_\mathrm{c}$ ($\lambda\tau \simeq (\lambda\tau)_\mathrm{c} + \delta\lambda\tau$), to lowest order, these solutions behave as

$$z_\pm(\lambda\tau) \simeq \pm i y_\mathrm{c} - \frac{e^{\mp i\gamma y_\mathrm{c}} + e^{\mp i y_\mathrm{c}}}{1 - \gamma(\lambda\tau)_\mathrm{c} e^{\mp i\gamma y_\mathrm{c}} - (\lambda\tau)_\mathrm{c} e^{\mp i y_\mathrm{c}}} \delta\lambda\tau \ , \tag{3.20}$$

where $y_\mathrm{c} = \frac{\pi}{1+\gamma}$. The dominant contributions for the scaling function as $\lambda\tau \rightarrow (\lambda\tau)_\mathrm{c}$ then come from the two terms in Eq. (3.10) when $(\alpha = \pm, \beta = \mp)$, yielding

$$\begin{aligned} f(\lambda\tau) &\simeq \frac{-8}{(1 - \gamma(\lambda\tau)_\mathrm{c} e^{-i\gamma y_\mathrm{c}} - (\lambda\tau)_\mathrm{c} e^{-i y_\mathrm{c}})(1 - \gamma(\lambda\tau)_\mathrm{c} e^{i\gamma y_\mathrm{c}} - (\lambda\tau)_\mathrm{c} e^{i y_\mathrm{c}})(z_+ + z_-)} \\ &= \frac{c_1(\gamma)}{(\lambda\tau)_\mathrm{c}(\gamma) - \lambda\tau} \ , \end{aligned} \tag{3.21}$$

where

$$c_1(\gamma) = \frac{4}{(1+\gamma)(\lambda\tau)_\mathrm{c} + (1+\gamma)(\lambda\tau)_\mathrm{c}\cos(\pi\frac{1-\gamma}{1+\gamma}) - \cos(\frac{\pi}{1+\gamma}) - \cos(\frac{\gamma\pi}{1+\gamma})} \ . \tag{3.22}$$

Finally, one can obtain the approximate scaling function for the full $0 < \lambda\tau <$

$(\lambda\tau)_c(\gamma)$ interval, using some heuristics following Ref. [67]. As can be observed in the numerical results in Fig. 3.2, the scaling function varies slowly between (and away from) the two singular points. Then, it can be approximated by

$$f(\lambda\tau) \simeq \frac{1}{\lambda\tau} + \frac{c_1(\gamma)}{(\lambda\tau)_c(\gamma) - \lambda\tau} + c_2(\gamma) \; . \tag{3.23}$$

In principle, the constant $c_2(\gamma)$ could be determined by matching the minimum value of the scaling function. Since it is not known analytically, instead one must resort to the heuristics of Ref.[67] where the constant $c_2(\gamma)$ is determined in such a way that it matches next-to-leading order corrections of the asymptotic behavior, e.g., near $\lambda\tau = 0$. To that end, the next-to-lowest order corrections to the solution of Eq. (3.16) in the vicinity of $\lambda\tau = 0$ are found to be

$$z(\lambda\tau) \simeq -2\lambda\tau - 2(1+\gamma)(\lambda\tau)^2 + \mathcal{O}((\lambda\tau)^3) \; . \tag{3.24}$$

Keeping the relevant orders in the dominant term in Eq. (3.10) gives

$$\begin{aligned} f(\lambda\tau) &\simeq \frac{-4}{(1-\gamma\lambda\tau-\lambda\tau)^2 \, 2(-2\lambda\tau - 2(1+\gamma)(\lambda\tau)^2)} \\ &\simeq \frac{1}{[1-(1+\gamma)\lambda\tau]^2 \lambda\tau(1+(1+\gamma)\lambda\tau)} \\ &\simeq \frac{1}{\lambda\tau} + (1+\gamma) \; . \end{aligned} \tag{3.25}$$

In order to match this next-to-leading order correction as $\lambda\tau \to 0$ with the proposed approximate scaling function Eq. (3.23), one must have

$$c_2(\gamma) = 1 + \gamma - \frac{c_1(\gamma)}{(\lambda\tau)_c(\gamma)} \; . \tag{3.26}$$

3.4 Special Cases

Having established the scaling theory for the phase boundary [Eq. (3.8)] and for the fluctuations [Eq. (3.14)], it is insightful to express the main findings explicitly in terms of the two types of delays appearing in the original formulation of the problem, Eq. (3.2). From Eq. (3.8), for the boundary of the synchronizable regime

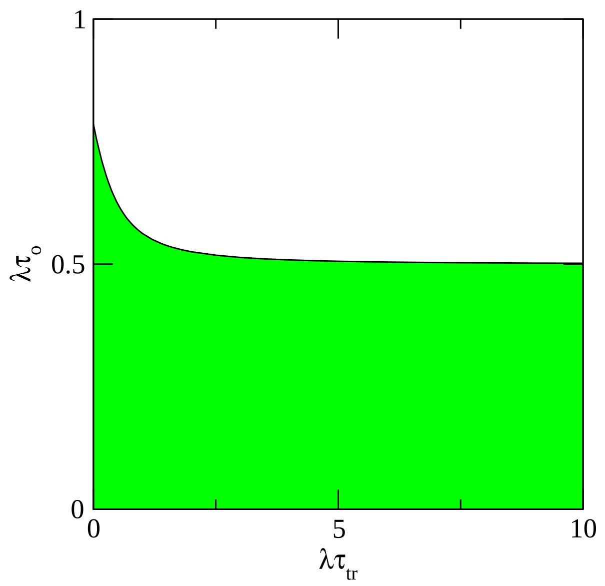

Figure 3.4: Synchronizability phase diagram on the $\lambda\tau_{\rm tr}$-$\lambda\tau_{\rm o}$ plane [Eq. (3.27)]. The shaded area indicates the synchronizable regime. The boundary of this region approaches the horizontal line $\lambda\tau_{\rm o} = 1/2$ in the limit of $\lambda\tau_{\rm tr} \to \infty$. Further, $\lambda\tau_{\rm o} = \pi/4$ when $\lambda\tau_{\rm tr} = 0$.

one immediately finds

$$\lambda(2\tau_{\rm o} + \tau_{\rm tr}) = \frac{\pi}{2}\sec\left(\frac{\pi}{2}\frac{\tau_{\rm tr}}{2\tau_{\rm o} + \tau_{\rm tr}}\right) . \tag{3.27}$$

While explicitly expressing the critical line $\tau_{\rm o}$ vs $\tau_{\rm tr}$ is prohibitive due to the implicit nature of Eq. (3.27), one can produce a plot for it numerically as in Fig. 3.4.

Further insight into the different impacts of the two types of delays by considering two limiting cases. First, consider the case when $\tau_{\rm o}/\tau_{\rm tr} << 1$, i.e., when the transmission delays are much larger than the local processing, cognitive, or execution delays. This is equivalent to the $\gamma << 1$ limit in the scaling expressions. From Eq. (3.8) one finds $(\lambda\tau)_{\rm c} \simeq 1/2\gamma$ or $(\lambda\tau_{\rm o})_{\rm c} = 1/2$. Thus, there is no singularity in the fluctuations for any finite $\tau_{\rm tr}$ provided that $\lambda\tau_{\rm o} < 1/2$. Further, from Eq. (3.14) (with the coefficients given in Section 3.3) for the steady-state fluctuations in the same limit we find

$$\langle u^2(\infty)\rangle \simeq \frac{D}{\lambda} + \left\{ \frac{4}{\pi^2}\frac{1}{1/2 - \lambda\tau_{\rm o}} + 1 - \frac{8}{\pi^2} \right\} \tau_{\rm tr} \; . \tag{3.28}$$

In the other limiting case, $\tau_{\rm tr}/\tau_{\rm o} << 1$, i.e., the transmission delays are much smaller than the local processing delays. This is equivalent to the $\gamma \to 1$ limit in our scaling expressions. In this limit Eq. (3.8) reduces to $(\lambda\tau_{\rm o})_{\rm c} = \pi/4$. The steady-state fluctuations approach

$$\langle u^2(\infty)\rangle \simeq \frac{D}{\lambda} + \left\{ \frac{4}{\pi}\frac{1}{\pi/4 - \lambda\tau_{\rm o}} + 2 - \frac{16}{\pi^2} \right\} \tau_{\rm o} \; , \tag{3.29}$$

provided that $\lambda\tau_{\rm o} < \pi/4$.

Figure 3.4 and Eqs. (3.28) and (3.29) highlight the subtle differences between the impacts of the two types of delays. The local delays $\tau_{\rm o}$ are the dominant ones, in that as long as $\lambda\tau_{\rm o} < 1/2$, there are no singularities for any finite $\tau_{\rm tr}$, and $\langle u^2(\infty)\rangle$ increases linearly with $\tau_{\rm tr}$ as $\tau_{\rm tr} \to \infty$ in accordance with Eq. (3.28). On the other hand, for every $\tau_{\rm tr}$, there is a sufficiently large $\tau_{\rm o}$ such that the fluctuations become singular. In particular, when the transmission delays are much smaller than the local processing delays, the fluctuations diverge as $\lambda\tau_{\rm o} \to \pi/4$, as is apparent from Eq. (3.29).

The above discussed synchronizability condition can also be rephrased in terms of the relevant time scales of the problem. The inverse of the effective coupling, $\tau_{\rm comm} \equiv \lambda^{-1}$, can be interpreted as the characteristic time between successive communications between system components (and the corresponding state adjustments using available "recent" information) [41, 61]. As shown above, $\tau_{\rm o}$ is the dominant delay in the availability of the information. For $\tau_{\rm comm}{>}2\tau_{\rm o}$, stability and synchronization is guaranteed. On the other hand, for $\tau_{\rm comm}{<}(4/\pi)\tau_{\rm o}$, synchronization cannot be achieved. Thus, attempting to communicate and adjust too frequently (limited by the availability of recent information), is not only useless, but will actually lead to complete desynchronization.

3.5 Application of Cauchy's Argument Principle with Implementation

Determining the stability of networks with two types of delay for system sizes greater than $N = 2$ requires numerical analysis. The following algorithm is a powerful tool in finding both the similarities and contrasts between the simple two-node system and more complex, interesting topologies. For an arbitrary complex analytic function $F(z)$, the number of zeros N_C inside a closed contour C (provided $F(z)$ has no poles/singularities inside C) is given by Cauchy's argument principle (see, e.g., Ref. [75]):

$$N_C = \frac{1}{2\pi i} \oint_C \frac{F'(z)}{F(z)} dz = \frac{1}{2\pi} \Delta_C \arg F(z) \ , \tag{3.30}$$

where $\Delta_C \arg F(z)$ is the winding number of $F(z)$ along the closed contour C. The characteristic equations studied in this thesis can all be written as a sum of exponentials, hence there are no singularities. The stability boundary is determined by following the methods of Refs. [76, 77], using Eq. (3.30) to track the number of zeros of the characteristic equations with positive real part (i.e., on the positive real half plane) by substituting Eqs. (3.49) and (3.55) for $F(z)$. The numerical algorithm was adopted directly from Reference [76], which determines the winding number with an adaptive step size. This method begins with a step of size h along the contour in the direction $\hat{\imath}$ from s to $s+h\hat{\imath}$. The step is accepted if $\theta(s, s+(h/2)\hat{\imath} < \theta(s, s+h\hat{\imath}) < \epsilon = 1$ where $\theta(s, s') \equiv |\arg(\det M(s)) - \arg(\det M(s'))| \bmod 2\pi$. The subsequent step size is then $h \to \max\{2, \epsilon/\Delta\}$; unacceptable steps are retried with $h \to h/2$. The winding number is the count of the number of crossings of π without a return in the opposite direction.

Choose the contour so that it detects the first zero to cross the imaginary axis and acquire a positive real part. Note that the mode corresponding to the zero eigenvalue allows the solution $z = 0$ for Eq. (3.50), so the zero at the origin must be actively ignored, e.g. by choosing the left edge of the contour to be nonzero but still very small. This method can be applied to any network structure with any delay scheme, provided the approximate general behavior of the zeros is understood.

For arbitrary couplings and delays, general properties of eigenvalues of com-

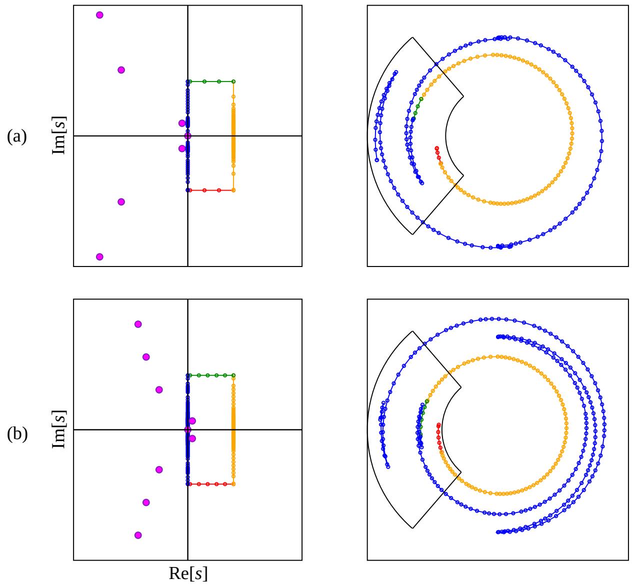

Figure 3.5: Numerical integration of Eq. (3.30) to identify the presence of zeros in the cases of a system of two coupled nodes ($\tau_c = \pi/4$) for (a) $\tau = \pi/5$ and (b) $\tau = \pi/3$. The left column shows the zeros and the points sampled along the contour; the right column shows the argument of the characteristic function (angular coordinate) at these steps (radial coordinate).

plex matrices can be utilized to bound the location of the eigenvalues, but smaller contours can be determined by building some intuition for a particular delay scheme. The height and width of the box are chosen after observing the general behavior of the location of zeros for representative networks. This is simple in the case of uniform time delay because the curves onto which all zeros fall have been well studied [2, 68]. The first zeros to acquire a positive real part will be on the curves with smallest imaginary parts. The width of the contour of integration must be great enough so that zeros that have acquired a positive real part are still included. Looking at the extreme cases of large system sizes and large delays, a reasonable limit can be chosen which will not overlook any zero but does not require an excessive amount of computation.

As an example, consider the simplest system of two coupled nodes with uniform delay, which has a critical delay of $\pi/4$. Figure 3.5 shows two cases explored while finding the critical delay. In Fig. 3.5(a), $\tau = \pi/5 < \tau_c$ and all real parts are non-positive so none fall within the contour. Tracking the argument (right column) shows that the winding number is correspondingly zero to verify that the delay is subcritical. Alternatively, $\tau = \pi/3 > \pi_c$ in Fig. 3.5(b) and there do indeed exist zeros with positive real parts that fall within the contour. The argument winds around the origin twice, signaling the presence of the first two zeros to cross the imaginary axis, indicating instability.

3.6 Fully Connected Networks

Consider the case of a fully connected network of size $N \geq 3$ with uniform link strengths σ, where the local state variables evolve according to

$$\begin{aligned}
\partial_t h_i(t) &= -\frac{\sigma}{N-1}\sum_{j\neq i}[h_i(t-\tau_o) - h_j(t-\tau)] + \eta_i(t) \\
&= -\frac{\sigma}{N-1}\sum_{j\neq i}[h_i(t-\gamma\tau) - h_j(t-\tau)] + \eta_i(t) \\
&= -\frac{\sigma}{N-1}\sum_{j\neq i}[h_i(t-\tau) - h_j(t-\tau)] + \sigma h_i(t-\tau) - \sigma h_i(t-\gamma\tau) + \eta_i(t) \\
&= -\frac{\sigma}{N-1}\sum_{j}\Gamma_{ij} h_j(t-\tau) + \sigma h_i(t-\tau) - \sigma h_i(t-\gamma\tau) + \eta_i(t) \qquad (3.31)
\end{aligned}$$

where $\tau \equiv \tau_{\mathrm{o}} + \tau_{\mathrm{tr}}$, $\gamma \equiv \tau_{\mathrm{o}}/\tau$ and $\Gamma_{ij} = \delta_{ij}N - 1$. Normalizing the global coupling with $1/(N-1)$ assures that the coupling cost per node remains constant and the region of synchronization remains finite in the limit of $N \to \infty$. This all-to-all coupling scheme abandons the restriction on the information of the system that is available to each node, since the local neighborhood has now become the entire network. However, as will be shown, the characteristics of the critical behavior of the system are very similar to that of a graph that is not fully connected, but the analysis is kept simpler and can be extended further. Using the fact that the graph Laplacian of the complete graphs has a single, nonzero eigenvalue N [which is $(N-1)$-fold degenerate], each non-uniform mode (associated with fluctuations about the mean) obeys

$$\partial_t \tilde{h}(t) = -\sigma \tilde{h}(t-\gamma\tau) - \frac{\sigma}{N-1}\tilde{h}(t-\tau) + \tilde{\eta}(t) \ . \tag{3.32}$$

As in the case of uniform delays, the characteristic polynomial and equation is determined by performing a Laplace transform on the deterministic part, yielding

$$g(s) \equiv s + \frac{\sigma}{N-1}e^{-\tau s} + \sigma e^{-\gamma\tau s} = 0 \ . \tag{3.33}$$

Note that for $N = 2$, the region of stability/synchronizability can be obtained analytically [66], and for completeness it is shown in Fig. 3.6 in the $(\tau_{\rm o}, \tau)$ plane. In this simple case of two coupled nodes, the synchronization boundary is monotonic, and the local delay is dominant: There is no singularity (for any finite $\tau_{\rm tr}$) as long as $\sigma\tau_o < 1/2$ [66], while for any $\tau_{\rm tr}$, there is a sufficiently large τ_o resulting in the breakdown of synchronization.

For $N \geq 3$, the phase diagram (region of synchronizability) can be obtained numerically by tracking the zeros of the characteristic equation Eq. (3.33) (i.e., identifying when their real parts switch sign) shown in Fig. 3.6. Note that keeping track of infinitely many complex zeros of the characteristic equations would be an insurmountable task. Instead, in order to identify the stability boundary of the system, one only needs to know whether *all* solutions have negative real parts. This test can be done by employing Cauchy's argument principle [76, 77] (see Section 3.5 for details). Similar to the N=2 case, the local delay is always dominant, i.e., there are critical values of $\sigma\tau_{\rm o}$ above/below which the system is unsynchronizable/synchronizable for any $\tau_{\rm tr}$. [These critical values approach $\pi/2$ as $N \to \infty$, since in this case Eqs. (3.32) and (3.33) reduce to the familiar forms of Eqs. (2.14) and (2.15), respectively, with the known analytic threshold.] The behavior with the overall delay $\tau = \tau_{\rm o} + \tau_{\rm tr}$, however, is more subtle: There is a range of τ_o where varying τ yields reentrant behavior with alternating synchronizable and unsynchronizable regions (as can be seen by considering suitably chosen horizontal cuts for fixed $\tau_{\rm o}$ in Fig. 3.6). Thus, in this region (for fixed local delays $\tau_{\rm o}$), stabilization of the system can also be achieved by *increasing* the transmission delays.

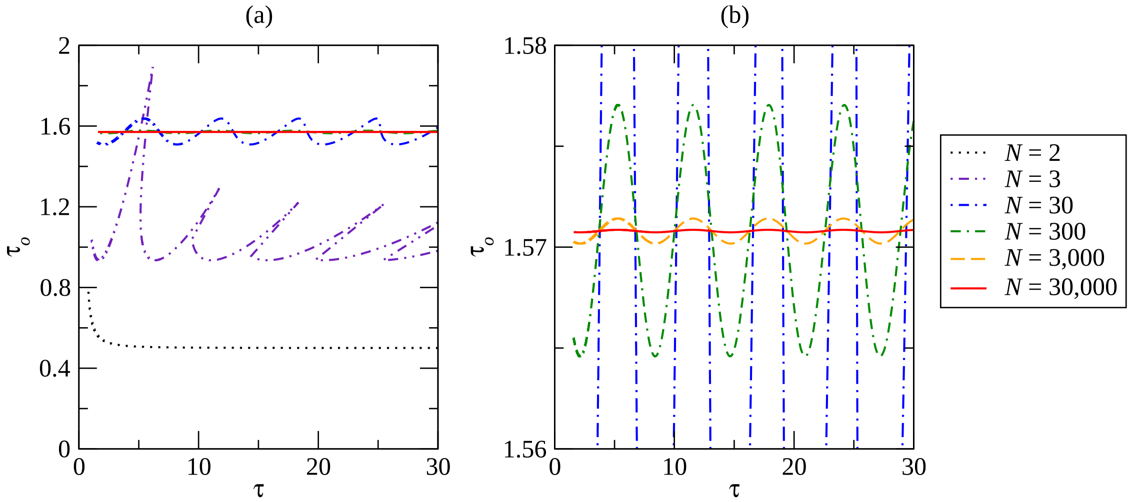

Figure 3.6: Phase diagram (synchronization boundary) for fully connected networks with uniform coupling strength $\sigma/(N-1)$ in the (τ_o, τ) plane. (Without loss of generality due to scaling, the scaling $\sigma = 1$ was used.) With the exception of the analytically solvable case of $N = 2$ [66], the synchronization boundaries, corresponding to stability limits, were obtained from the analysis of the zeros of Eq. (3.33).

In the special case $\gamma = 0$, the network is always synchronizable for all N and the width can be obtained exactly (see Section 2.3.2.b),

$$\langle w^2(\infty)\rangle = \frac{1}{N}\sum_{k=1}^{N-1}\langle \tilde{h}_k^2(\infty)\rangle = \frac{D(N-1)}{N}\,\frac{\alpha + \frac{\sigma}{N-1}\sinh(\alpha\tau)}{\alpha[\sigma + \frac{\sigma}{N-1}\cosh(\alpha\tau)]} \tag{3.34}$$

with $\alpha = \sigma\sqrt{1 - 1/(N-1)^2}$, as shown in Fig. 3.7. For $\tau = \tau_{\mathrm{tr}} \to \infty$, the above expression becomes

$$\langle w^2(\infty)\rangle = \frac{D(N-1)}{N}\,\frac{1}{\sigma\sqrt{1 - 1/(N-1)^2}}\ . \tag{3.35}$$

3.7 The Uniform Mode and the Width

3.7.1 Eigenmode Decomposition

In synchronization and coordination problems, it is natural to define an observable such as the width, which measures fluctuations with respect to the global

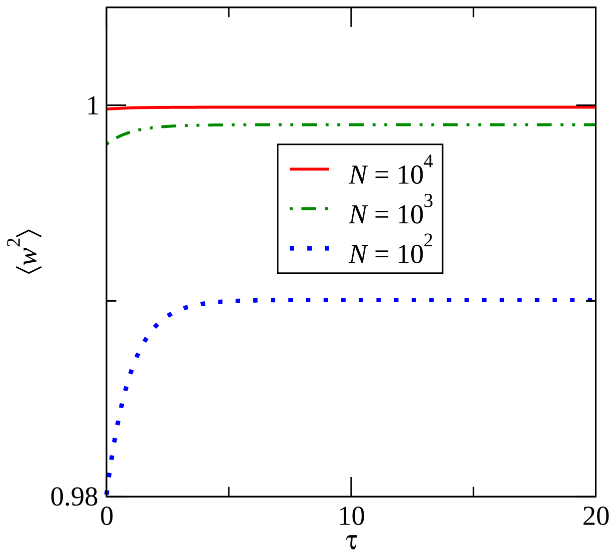

Figure 3.7: Analytic results for stationary-state widths for fully connected networks of several sizes for the special case $\gamma = 0$ [Eq. (3.34)]. Here, $D = 1$ and $\sigma = 1$.

mean,

$$w^2(t) = \frac{1}{N}\sum_{i=1}^{N}[h_i(t) - \bar{h}(t)]^2 , \tag{3.36}$$

where $\bar{h}(t) = \sum_{i=1}^{N} h_i(t)$. The amplitude associated with the uniform mode of the normalized Laplacian automatically drops out from the width. (In the case of unnormalized symmetric coupling, the expression for the width simplifies to the known form.)

For the problem with two types of time delays and locally normalized couplings as in Eq. (3.47), decomposition along the right eigenvectors of $K^{-1}L$ facilitates diagonalization. While this normalized Laplacian is a non-symmetric matrix, its eigenvalues are all real and non-negative (with the smallest being zero, $\lambda_0 = 0$). The corresponding (normalized) right eigenvector is

$$|e_0\rangle = N^{-1/2}(1, 1, \ldots, 1)^T . \tag{3.37}$$

Note that since the normalized Laplacian is non-symmetric, the eigenvectors are not orthogonal, i.e., $\langle e_l|e_k\rangle \neq \delta_{lk}$. To ease notational burden, this subsection uses the bra-ket notation – not to be confused with ensemble average over the noise. In this notation, $\langle\cdot|$ is a row vector and $|\cdot\rangle$ is a column vector, e.g., $\langle e_0| = N^{-1/2}(1, 1, \ldots, 1)$. Using this notation, the state vector is denoted by

$$|h(t)\rangle = (h_1(t), h_2(t), \ldots, h_N(t))^T \ , \tag{3.38}$$

while the state vector relative to the mean is

$$\begin{aligned}
|h(t) - \bar{h}(t)\rangle &= (h_1(t) - \bar{h}(t), h_2(t) - \bar{h}(t), \ldots, h_N(t) - \bar{h}(t))^T \\
&= (h_1(t), h_2(t), \ldots, h_N(t))^T - \bar{h}(t)(1, 1, \ldots, 1)^T \\
&= |h(t)\rangle - \bar{h}(t)\sqrt{N}|e_0\rangle = (1 - |e_0\rangle\langle e_0|)|h(t)\rangle \ .
\end{aligned} \tag{3.39}$$

Employing the above formalism, the width can be written as

$$w^2(t) = \frac{1}{N}\sum_{i=1}^{N}[h_i(t) - \bar{h}(t)]^2 = \frac{1}{N}\langle h - \bar{h}|h - \bar{h}\rangle \ . \tag{3.40}$$

Now the state vector can be expressed as the linear combination of the eigenvectors of the underlying Laplacian,

$$|h(t)\rangle \sum_{k=0}^{N-1} \tilde{h}_k(t)|e_k\rangle \ . \tag{3.41}$$

Employing the above eigenmode decomposition, $\langle h-\bar{h}|h-\bar{h}\rangle$ can be written as

$$\begin{aligned}
\langle h-\bar{h}|h-\bar{h}\rangle &= \langle h|(1-|e_0\rangle\langle e_0|)^2|h\rangle = \langle h|(1-|e_0\rangle\langle e_0|)|h\rangle \\
&= \sum_{k=0}^{N-1}\tilde{h}_k(t)\langle e_k|\left(1-|e_0\rangle\langle e_0|\right)|\sum_{l=0}^{N-1}\tilde{h}_l(t)|e_l\rangle \\
&= \sum_{k,l=0}^{N-1}\tilde{h}_k(t)\tilde{h}_l(t)\langle e_k|\left(1-|e_0\rangle\langle e_0|\right)|e_l\rangle \\
&= \sum_{k,l=0}^{N-1}\tilde{h}_k(t)\tilde{h}_l(t)\left(\langle e_k|e_l\rangle-\langle e_k|e_0\rangle\langle e_0|e_l\rangle\right) \\
&= \sum_{k,l\neq 0}\tilde{h}_k(t)\tilde{h}_l(t)\left(\langle e_k|e_l\rangle-\langle e_k|e_0\rangle\langle e_0|e_l\rangle\right) \\
&= \sum_{k,l\neq 0}\tilde{h}_k(t)\tilde{h}_l(t)\left(E_{kl}-E_{k0}E_{0l}\right)\ , \qquad (3.42)
\end{aligned}$$

where $E_{kl}\equiv\langle e_k|e_l\rangle$. As can be seen explicitly from Eq. (3.42), the terms where either k or l are zero drop out from the sum (as E_{00}=1). It is also clear from Eq. (3.42) that $\langle h-\bar{h}|h-\bar{h}\rangle=\sum_{k\neq 0}\tilde{h}_k^2(t)$ when the underlying coupling is symmetric (and consequently the eigenvectors form an orthogonal set, E_{kl}=δ_{kl}). Finally, the width can be written as

$$\begin{aligned}
w^2(t) &= \frac{1}{N}\sum_{i=1}^{N}[h_i(t)-\bar{h}(t)]^2 = \frac{1}{N}\langle h-\bar{h}|h-\bar{h}\rangle \\
&= \frac{1}{N}\sum_{k,l\neq 0}\tilde{h}_k(t)\tilde{h}_l(t)\left(E_{kl}-E_{k0}E_{0l}\right)\ . \qquad (3.43)
\end{aligned}$$

Note that the above result can be immediately applied to the case of symmetric coupling with no transmission delays in Eq. (2.1). There, the eigenvectors of the corresponding Laplacian form an orthogonal set, and the above expression collapses to $w^2(t)=\frac{1}{N}\sum_{k=1}^{N-1}\tilde{h}_k^2(t)$ [61].

3.7.2 Ensemble Average over the Noise

Using the general form of the solution given by Eq. (2.10) for the respective eigenmodes of normalized Laplacian coupling with two types of time delays

[Eq. (3.48)] gives

$$\tilde{h}_k(t) = \int_0^t dt' \sum_\alpha \frac{e^{s_{k\alpha}(t-t')}}{g_k'(s_{k\alpha})} \tilde{\eta}_k(t') \; , \tag{3.44}$$

where $s_{k\alpha}$ is the αth solution of the kth mode for the characteristic equation $g_k(s) = 0$ from Eq. (3.49). After averaging over the noise, one obtains for the two-point function

$$\langle \tilde{h}_k(t)\tilde{h}_l(t)\rangle = -2D\chi_{kl} \sum_{\alpha,\beta} \frac{(1 - e^{(s_{k\alpha}+s_{l\beta})t})}{g_k'(s_{k\alpha})g_l'(s_{l\beta})(s_{k\alpha}+s_{l\beta})} \; . \tag{3.45}$$

In the stationary state, one must have $\mathrm{Re}(s_{k\alpha}) < 0$ for all k and α. Thus, the stationary state width can be written as

$$\begin{aligned} \langle w^2(\infty)\rangle &= \lim_{t\to\infty} \frac{1}{N} \sum_{k,l\neq 0} \langle \tilde{h}_k(t)\tilde{h}_l(t)\rangle \, (E_{kl} - E_{k0}E_{0l}) \\ &= \frac{-2D}{N} \sum_{k,l\neq 0} \sum_{\alpha,\beta} \frac{(E_{kl} - E_{k0}E_{0l})\,\chi_{kl}}{g_k'(s_{k\alpha})g_l'(s_{l\beta})(s_{k\alpha}+s_{l\beta})} \; . \end{aligned} \tag{3.46}$$

3.8 Locally Weighted Networks

Now consider Eq. (3.1) with specific locally weighted couplings (already utilized for uniform local time delays in Section 2.7), $C_{ij} = \sigma A_{ij}/k_i$. The set of differential equations then have the form

$$\begin{aligned} \partial_t h_i(t) &= -\frac{\sigma}{k_i} \sum_j A_{ij}[h_i(t-\gamma\tau) - h_j(t-\tau)] + \eta_i(t) \\ &= -\frac{\sigma}{k_i} \sum_j L_{ij} h_j(t-\tau) + \sigma h_i(t-\tau) - \sigma h_i(t-\gamma\tau) + \eta_i(t) \\ &= -\sigma \sum_j \Gamma_{ij} h_j(t-\tau) + \sigma h_i(t-\tau) - \sigma h_i(t-\gamma\tau) + \eta_i(t) \; , \end{aligned} \tag{3.47}$$

where σ controls the coupling strength and $\Gamma = K^{-1}L$ is now the locally weighted network Laplacian ($K_{ij} = \delta_{ij}k_i$, and $L_{ij} = \delta_{ij}\sum_l A_{il} - A_{ij} = \delta_{ij}k_i - A_{ij}$). Diagonalization yields

$$\partial_t \tilde{h}_k(t) = \sigma(1-\lambda_k)\tilde{h}_k(t-\tau) - \sigma\tilde{h}_k(t-\gamma\tau) + \tilde{\eta}_k(t) \tag{3.48}$$

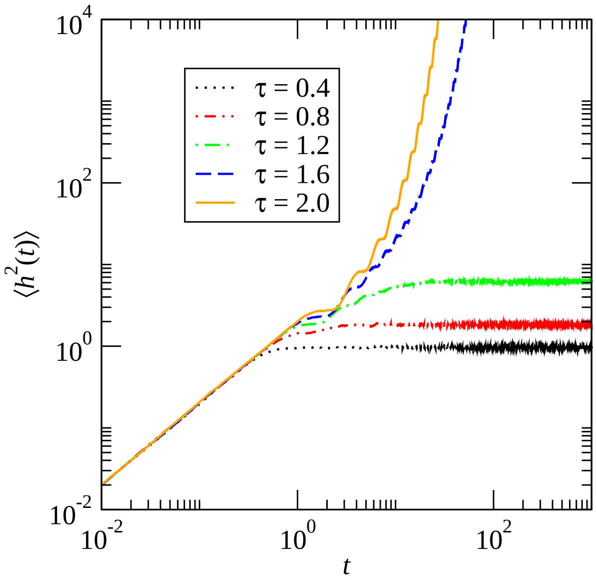

Figure 3.8: Time series of the fluctuations of a single mode for several delays obtained from numerical integration of Eq. (3.48) with γ=0.5, λ=1.8, D=1, and Δt=0.01, averaged over 10^3 realizations of the noise ensemble.

where λ_k is the eigenvalue of the kth mode of the normalized graph Laplacian $K^{-1}L$. Figure 3.8 shows the evolutions of a particular mode with delays on either side of the critical delay. The characterisitic equation for the kth mode is then

$$g_k(s) = s + \sigma(\lambda_k - 1)e^{-\tau s} + \sigma e^{-\gamma\tau s} = 0\ . \tag{3.49}$$

Defining the new scaled variable $z = \tau s$, this equation becomes

$$z + (\sigma\tau)(\lambda_k - 1)e^{-z} + (\sigma\tau)e^{-\gamma z} = 0\ . \tag{3.50}$$

Hence, the solutions of the original characteristic equation depends on σ and τ in the form of $s_{k\alpha} = \tau^{-1}z_{k\alpha}(\sigma\tau)$. Although the scaling function of the width in the case of locally normalized couplings with two time delays cannot be expressed in a closed form, the general scaling behavior is identical to Eq. (2.55) [as follows from the formal solution shown in Section 3.7, Eq. (3.46)], i.e., $\langle w^2(\infty)\rangle_{\sigma,\tau} = D\tau F(\sigma\tau)$. The corresponding scaling behavior and scaling collapse, obtained from numerical

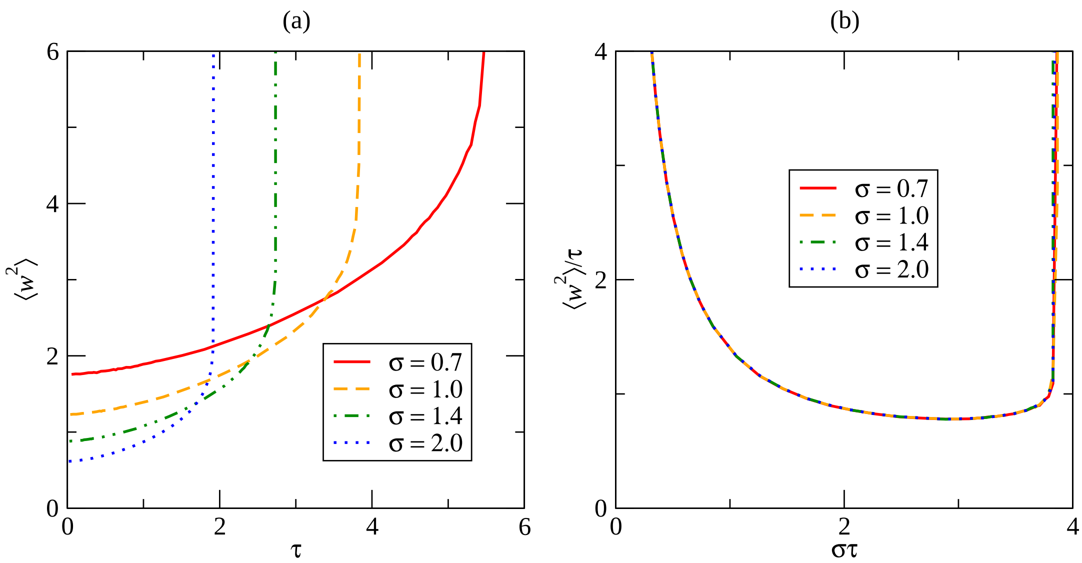

Figure 3.9: Comparison of (a) the widths and (b) the scaled widths for several coupling strengths σ on a typical locally weighted BA network of size $N = 100$ and $\langle k \rangle \approx 6$ for $\gamma = 0.2$; simulated with $D = 1$ and $\Delta t = 0.001$.

integration of Eq. (3.47), are shown in Fig. 3.9.

The stability/synchronization boundary was again determined by employing Cauchy's argument principle [76, 77], applied separately for each mode (Section 3.5). Figure 3.10 shows the most important eigenvalues to determine synchronizability: the greatest restriction to the critical delay $\tau_c = (\tau_o + \tau_{tr})_c$ for a given γ belongs to either the smallest or largest eigenvalues. An alternative presentation is given in Fig. 3.11, which shows that it is not always the same eigenvalue that consistently limits synchronizability for all values of γ; rather it is the eigenvalue that falls on the lowest point on the boundary curve. The contributions of a few example modes to the width are shown in Fig. 3.12(a). Note that the order of divergences is not the same as the ordered eigenvalues, in accordance with Fig. 3.10. The contributions of a single mode for various values of γ is shown in Fig. 3.12(b). Since it is τ_o that has a greater impact on whether or not a network can synchronize, larger total delays τ are tolerated for smaller γ since more of the delay comes from transmission. Because of the great sensitivity of $\langle h^2 \rangle$ on Δt near the divergence for longer delays,

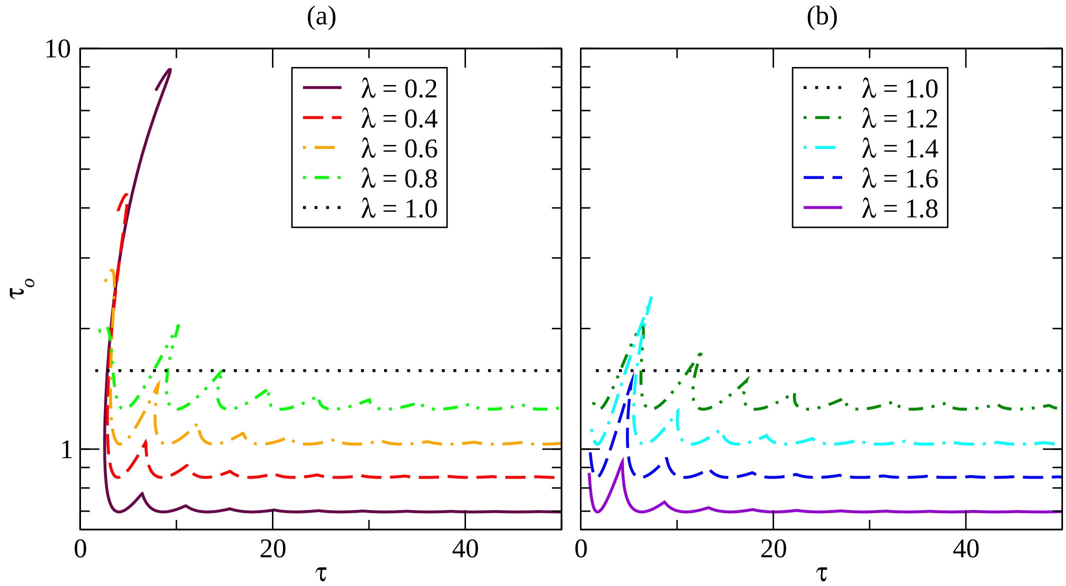

Figure 3.10: Synchronization boundaries for several modes with (a) $\lambda_k \leq 1$ and (b) $\lambda_k \geq 1$ of a weighted network, obeying Eq. (3.48) and determined by analyzing the zeros of Eq. (3.50).

an adaptive algorithm was implemented, which would halve Δt until consecutive runs agreed within 1%.

With this understanding of the underlying modes, let us return to synchronization of the entire system. Incorporating all relevant eigenvalues results in the synchronization boundary shown in Fig. 3.13(a) for several representative networks. The cut for a carefully chosen local delay in Fig. 3.13(b) shows the previously mentioned reentrant behavior as the transmission delay is increased. Note that the optimal width within each synchronizable region worsens with larger delay, so that while synchronizability can be recovered with increasing τ_{tr}, better synchronization is possible by decreasing τ_{tr}. To compare the contribution of modes within the synchronizable regime, consider again the two topologies of BA and ER graphs. For fixed γ, Fig. 3.14 shows that a BA graph remains synchronizable for larger delays than a ER graph when the link strengths are weighted by node degree. However, the ER graph synchronizes slightly better for the majority of the time that it is synchronizable. Here it is not the topology but the ratio γ that has the most drastic

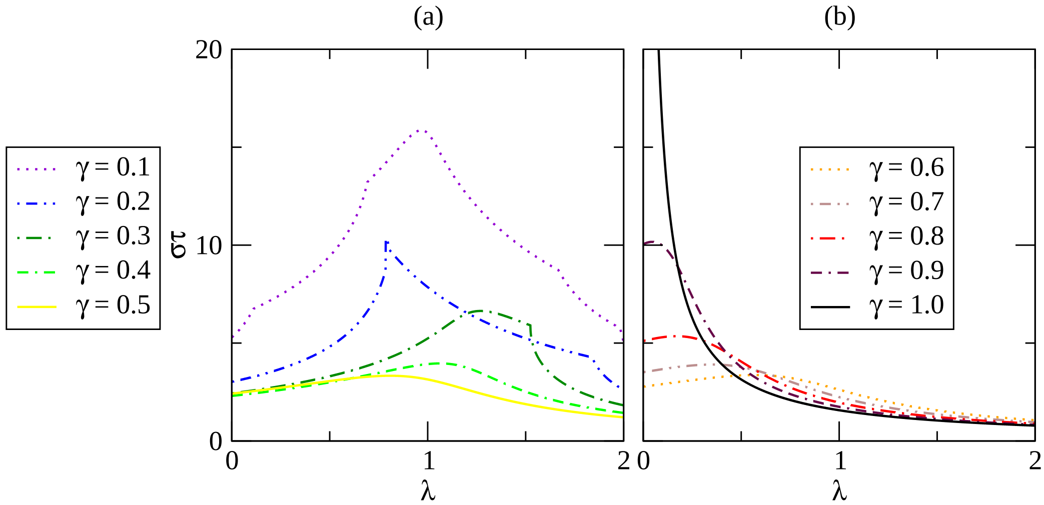

Figure 3.11: Synchronization boundaries determined by analyzing the zeros of Eq. (3.50) for various delay ratios γ, segregated with (a) $\gamma \leq 0.5$ and (b) $\gamma \geq 0.6$.

effect.

When $\gamma < 1$, the mode corresponding to $\lambda_0 = 0$ includes self-interaction terms and has the critical delay

$$\tau_c(\lambda = 0) = \frac{\pi}{1+\gamma}\left|\sec\left(\pi\frac{1-\gamma}{1+\gamma}\right)\right|. \tag{3.51}$$

While the uniform mode does not contribute to the width because $\bar{h}$ is removed from the state of the network (see Section 3.7), a diverging mean can introduce egregious truncation errors into the numerical integration if $\bar{h}$ diverges exponentially while the width remains finite. Fortunately, this can be avoided by simulating the network in the subspace lacking the zero mode by removing the mean from each time slice. Since the uniform mode is not allowed propagate, it does not cause any problem with finite precision. The locations of the zeros' real parts for Eq. (3.50) are tracked again using Cauchy's argument principle (see Section 3.5).

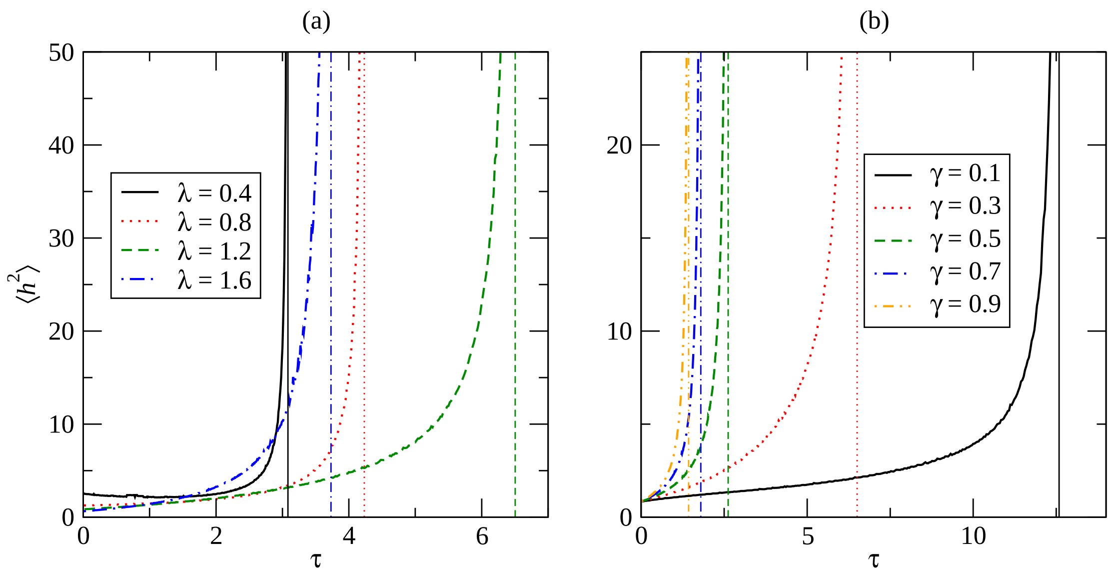

Figure 3.12: Width contributions for (a) several modes with $\gamma = 0.3$ and (b) several delay ratios with $\lambda = 1.2$, found by numerically integrating Eq. (3.48) with D=1 and σ=1. The vertical lines correspond to the stability limits obtained from the analyses of the zeros of Eq. (3.49) with the same λ.

3.9 Arbitrary Couplings and Multiple Delays

When there are multiple time delays involved in the synchronization or coordination process, in general, one cannot diagonalize the underlying system of coupled equations. This happens to be the case for the scenario with two types of time delay [Eq. (3.1)] on *unweighted* (or globally weighted) graphs (as opposed to specific locally-weighted ones discussed in Section 3.8). The effects of heterogeneous or distributed delays have been considered previously for their benefits to synchronization [78, 79]. A generally applicable method to determine the region of synchronizability/stability computationally can be derived by following the method from Refs. [76, 77]. For arbitrary couplings C_{ij}, the deterministic part of Eq. (3.1) (from which one can extract the characteristic equation) becomes

$$\partial_t h_i(t) = -C_i h_i(t - \tau_o) + \sum_j C_{ij} h_j(t - \tau) , \tag{3.52}$$

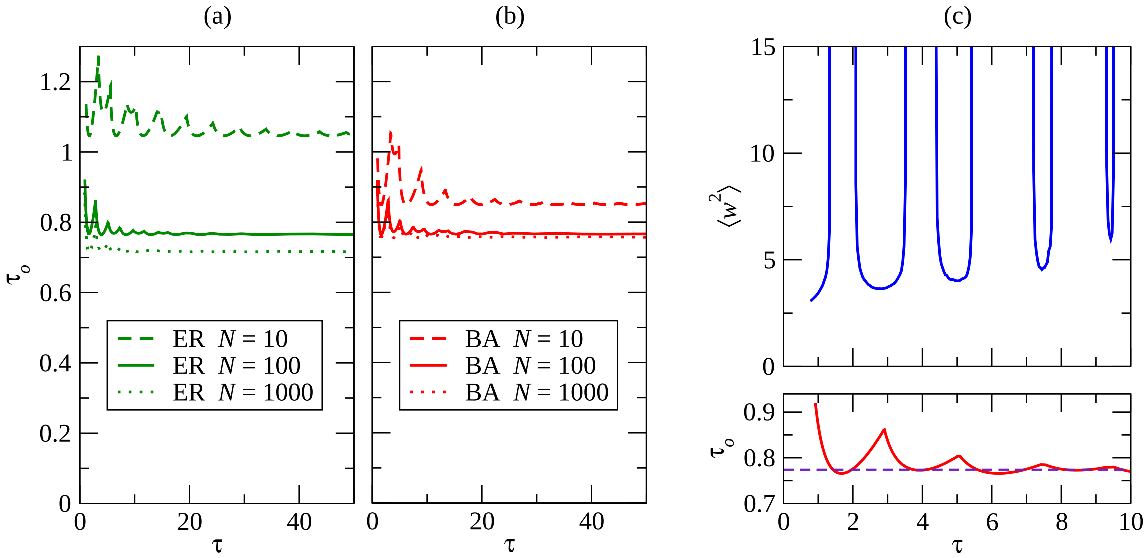

Figure 3.13: Synchronization boundaries for typical (a) ER and (b) BA networks of several sizes with locally weighted couplings. The boundaries are found by numerical diagonalization and examining each mode through Eq. (3.49). (c) Widths along a slice of constant τ_o=0.77 for the same N=100 BA network used in (b). For stability comparison, the boundary is shown below with the slice indicated.

where $C_i = \sum_l C_{il}$ and $\tau = \tau_\mathrm{o} + \tau_\mathrm{tr}$. After Laplace transform, these equations become

$$s\hat{h}_i(s) = -C_i\hat{h}_i(s)e^{-s\tau_\mathrm{o}} + \sum_j C_{ij}\hat{h}_j(s)e^{-s\tau} \;, \tag{3.53}$$

or equivalently,

$$\sum_j \left(s\delta_{ij} + C_i\delta_{ij}e^{-s\tau_\mathrm{o}} - C_{ij}e^{-s\tau}\right)\hat{h}_j(s) = 0 \;. \tag{3.54}$$

Hence, non-trivial solutions of the above system of equations require

$$\det M(s) = 0 \;, \tag{3.55}$$

where

$$M_{ij}(s) = s\delta_{ij} + C_i e^{-s\tau_\mathrm{o}}\delta_{ij} - C_{ij}e^{-s\tau} \;. \tag{3.56}$$

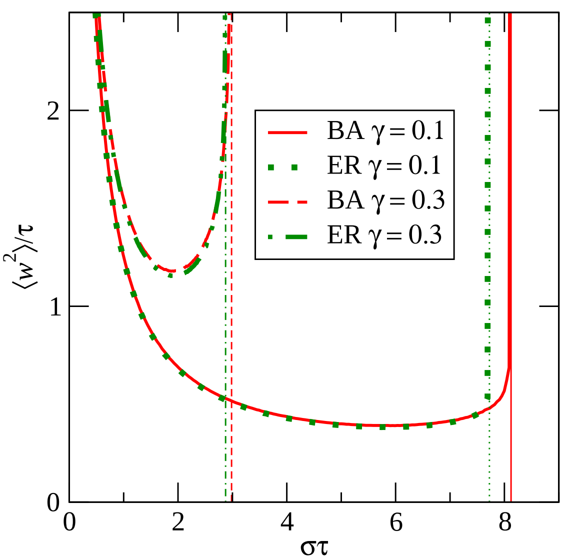

Figure 3.14: The scaling functions of a typical locally weighted BA network and a typical ER network for two delay ratios, with both networks of size N=100, found by numerically integrating Eq. (3.47) with D=1 and Δt=0.001. The vertical lines correspond to the stability limits obtained from the analyses of the zeros of Eqs. (3.50).

Stability or synchronizability requires that $\mathrm{Re}(s) < 0$ for *all* solutions of the above (transcendental) characteristic equation [Eq. (3.55)]. To identify the stability boundary of this coupled system, one does not need to know and determine the (infinitely many) complex solutions of the characteristic equation, but only whether all solutions have negative real parts. To test that, one again can employ the argument principle [76, 77] (Section 3.5). Note that the above method can be immediately generalized to arbitrary heterogeneous (local and transmission) time delays. To compare synchronizability with locally weighted couplings of the same cost as in Eq. (3.47), now consider the couplings $C_{ij} = \sigma A_{ij}/\langle k \rangle$. The results are shown in Fig. 3.15. The synchronization boundary was determined using the above scheme, while the width was obtain by numerically integrating Eq. (3.1). Not only does local reweighting of the coupling strength improve synchronization, but it also *extends* the region of synchronizability.

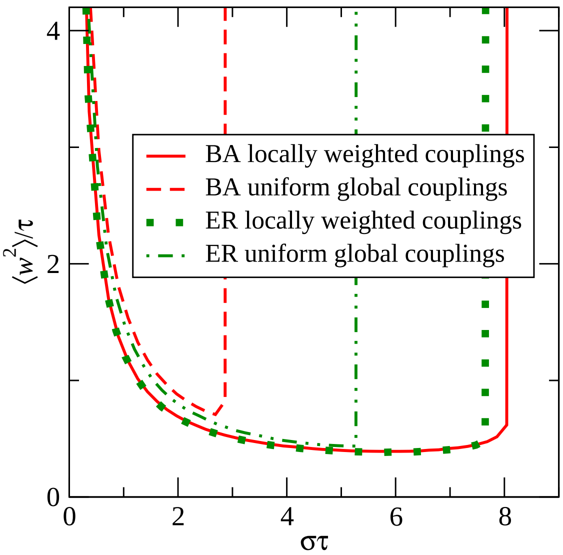

Figure 3.15: Scaled width curves for a typical BA network compared to those of a typical ER network of size $N = 100$ with $\langle k \rangle \approx 6$ and $D = 1$, determined by numerically integrating Eq. (3.1) for the two types of coupling schemes with $\gamma = 0.1$ and $\Delta t = 0.01$.

CHAPTER 4
Extreme Fluctuations in Networks with Time Delays

Along with the average fluctuations about the steady state given by the width, knowledge of the extreme values of the fluctuations can be useful for gauging the behavior of a network. Extremes have been of special interest in situations of surface growth [80] and parallel discrete-event simulations [81], and have already been studied in networks with no time delay [81, 44, 82]. To examine these extremes, consider the quantity $\Delta_{\max} \equiv \max\{h_i - \bar{h}\}_i$. Because of the symmetry of the relaxation behavior with regard to being above or below the mean, the distribution of $\Delta_{\max}$ is the same as that for $\Delta_{\min} \equiv \max\{\bar{h} - h_i\}_i$ and consequently simply related to $\Delta \equiv \Delta_{\max} + \Delta_{\min}$.

4.1 Statistics

The scaling behavior of extreme fluctuations in the case of no time delay has been investigated previously for SW [81] and SF networks [44, 82]. The established derivation of the expected distributions of extremes is also applicable to the case of nonzero time delay [81], so for completeness I adopt that notation and include it here.

To begin, consider a set of N independent and identically distributed random variables $\{\Delta_i\}_{i=1}^{N}$. Such a scenario can be applied to a large system that has many random connections because the correlations between nodes decay quickly for more distant nodes, so that widely separated nodes are effectively uncorrelated. Denote the probability for any one of these variables to be greater than x by $P_>(x)$. Assume that

$$P_>(x) \simeq e^{-cx^\delta} \tag{4.1}$$

for x large and with c and δ constants. Since the noise is Gaussian and the couplings are linear, it is expected that $\delta = 2$. The probability that the variable is less than x is related by $P_<(x) = 1 - P_>(x)$. The distribution for the largest value being less than x can then be expressed as

$$P^{\max}_{<}(x) = [P_{<}(x)]^N = [1 - P_{>}(x)]^N. \tag{4.2}$$

Inserting Eq. (4.1) and employing the convenient identity $\log(1+a) \approx a$ for $a \ll 1$ yields

$$P^{\max}_{<}(x) = e^{N \ln([1-P_{>}(x)])} \simeq e^{-NP_{>}(x)} = e^{-e^{cx^{\delta}+\ln N}}. \tag{4.3}$$

This distribution can be rescaled by $\tilde{x} = (x - a_N)/b_N$ to the Fisher-Tippett-Gumbel (FTG) distribution [81, 83, 84, 85] so that

$$\tilde{P}^{\max}_{<}(\tilde{x}) \simeq e^{-e^{-\tilde{x}}} \tag{4.4}$$

by the extreme-value limit theorem. This distribution can again be rescaled for zero mean and unit variance (removing the mean $\langle\tilde{x}\rangle = \gamma$, the Euler constant, and scaling the variance $\sigma^2_{\tilde{x}} = \pi^2/6$ of the FTG distribution) so that a comparison across various network sizes and delays is convenient. This alternate scaled extreme with zero mean and unit variance is related to $\Delta_{\max}$ by

$$y \equiv (\Delta_{\max} - \langle\Delta_{\max}\rangle)/\sigma_{\Delta_{\max}}. \tag{4.5}$$

Continuing with the derivation from [81],the expected largest value is given by

$$\langle x_{\max}\rangle = a_N + b_N\gamma \approx \left[\frac{\ln N}{c}\right]^{1/\delta} + (\delta c)^{-1}\left[\frac{\ln N}{c}\right]^{(1/\delta)-1}\gamma \sim \left[\frac{\ln N}{c}\right]^{1/\delta} \tag{4.6}$$

to leading order with $\mathcal{O}(1/\ln N)$ corrections. These corrections will be noticeable in the network sizes that will be considered.

4.2 Scaling with Uniform Delay

As an initial investigation into the effect of time delay on $\Delta_{\max}$, consider the simplest case of nonzero time delay as in Chapter 2. Through numerical integration of Eq. (2.1) and monitoring $\Delta_{\max}$ at each time step, a distribution can be constructed for the extreme fluctiations. Increasing the delay shifts the average of

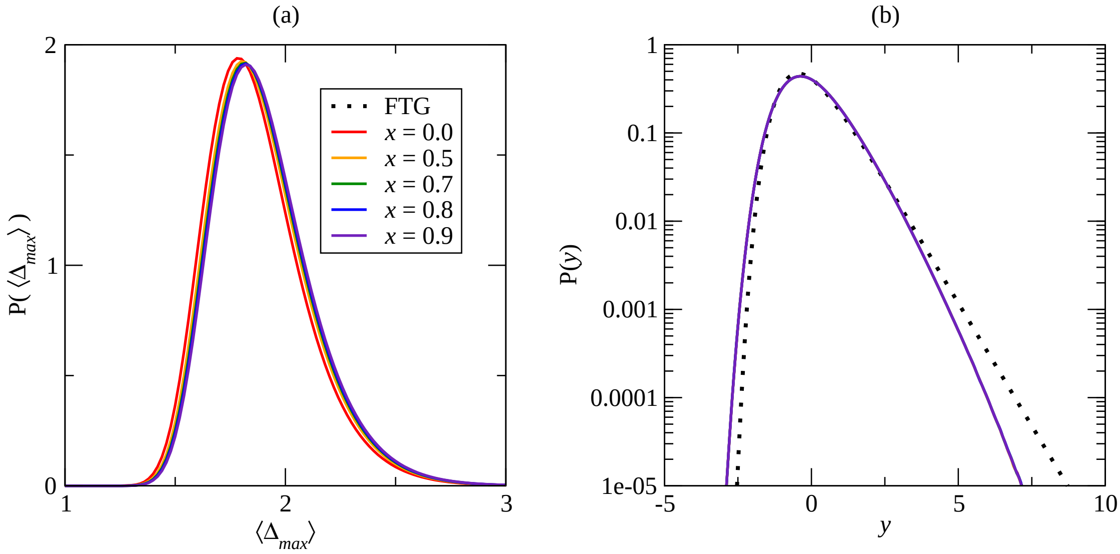

Figure 4.1: (a) Extreme fluctuation distributions for various delays for a typical BA network with $N = 10^3$, produced by numerically integrating Eq. (2.1) with $\Delta t = 0.001$. (b) Rescaling of (a) according to Eq. 4.5.

the distribution higher, but does not significantly alter the shape, as shown in Fig. 4.1(a). The parameter x here is the fraction of the critical delay for the network. Figure 4.1(b) shows that the same FTG distribution from zero time delay also approximates the rescaled widths when nonzero delays are present. Similarly, 4.2 shows the same two plots for a typical ER network. While the BA network distributions become wider as the delay is increased (and hence the peak becomes lower), the ER network exhibits a narrowing of the distribution. In other words, a larger time delay does not only lead to more extreme fluctuations in ER networks, but also to more consistently large extremes. A progression of distributions showing the approach to the FTG distribution is shown in Fig. 4.3. The corrections of $\mathcal{O}(1/\ln N)$ vanish slowly and are expected to be noticeable for these somewhat small system sizes.

The displacement of individual nodes (Δ_i) can change drastically as the critical delay is approached. Specifically, the highest degree nodes synchronize the best (i.e., have the narrowest distribution about zero for Δ_i) when the delay is well below the critical delay. The $1/k$-dependence of Δ_i (in accord with [15]) is shown in Fig. 4.4

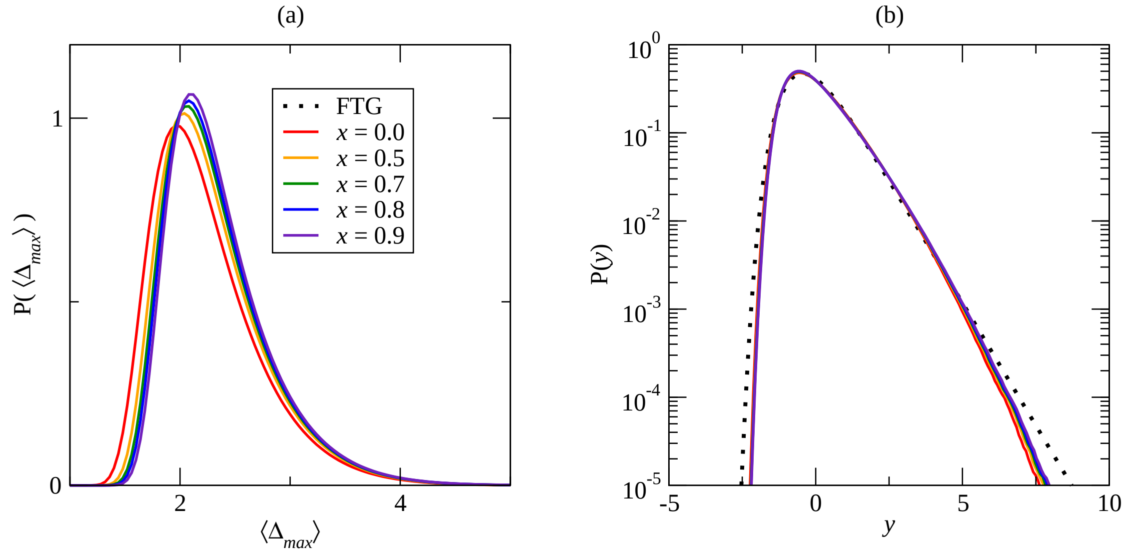

Figure 4.2: (a) Extreme fluctuation distributions for various delays for a typical ER network with $N = 10^3$, produced by numerically integrating Eq. (2.1) with $\Delta t = 0.001$. (b) Rescaling of (a) according to Eq. 4.5.

by a dotted line. However, as the delay increases, these hub nodes become the worst-synchronized nodes in the network as the oscillations become more sustained locally about them. The displacement of individual nodes Δ_i has a Gaussian distribution. In agreement with Fig. 4.4, the spread of Δ_i is hardly affected by the presence of a time delay, even at 95% of τ_c (see Fig. 4.5). However, there is a noticeable change for a node of intermediate degree and a very significant spreading of Δ_i (i.e., the node is poorly synchronized) for the highest degree node.

In order to consider the scaling behavior of $\Delta_{\max}$ for ensembles of networks of a given size, let us look at $\langle\Delta_{\max}\rangle$, the highest displacement of any node when the system is in the steady state averaged over a random ensemble of networks. The delay is constant across all networks of the same size, but varies on N according to the average critical delay for *all* networks of size N. To be explicit, this method requires taking an ensemble (10^4) of random networks of a given size and determining the average largest eigenvalue. The delay for each ensemble of size N is then a fraction x of the critical delay, with this fraction held constant over all network

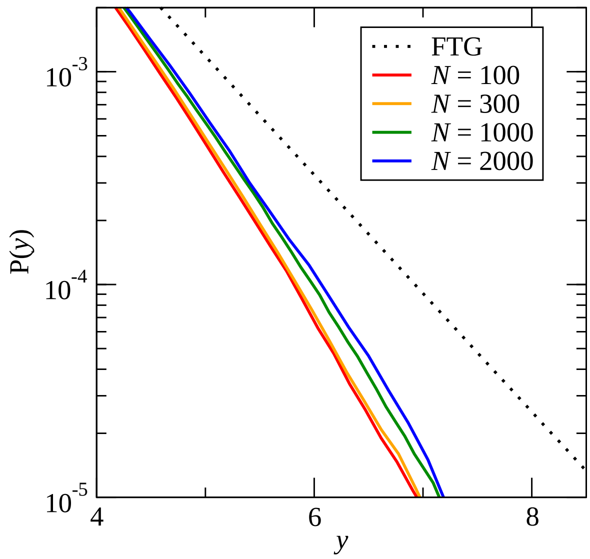

Figure 4.3: Extreme fluctuation distributions produced identically as in Fig. 4.1, for BA networks of several sizes for $x = 0.9$ to show the approach to the FTG distribution. Note the focus on y [Eq. 4.5] values to make the trend better visible.

sizes. Only networks which are synchronizable for the given delay (as discussed in Section 2.5) are included in the computation for $\langle\Delta_{\max}\rangle$. The results for typical BA networks are shown in Fig. 4.6(a), while those for typical ER networks are shown in Fig. 4.6(b). Both networks exhibit the expected scaling dependence on $\ln N$, although larger system sizes must be considered in order for the exact scaling to manifest.

The natural continuation of this particular line of investigation concerning extreme fluctuations would involve generalizations. The most straight-forward approach would resemble those generalizations explored for the width, which include various topologies and weightings as well and multiple time delays.

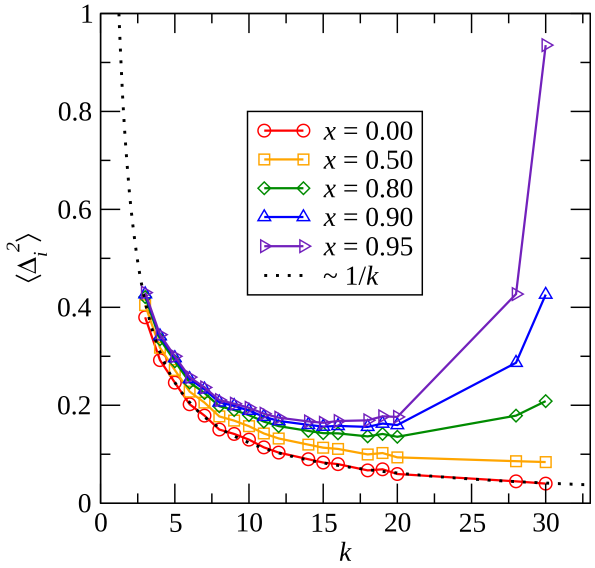

Figure 4.4: Fluctuations of individual nodes for a typical BA network of size $N = 100$ for various delay fractions x, produced by numerically integrating Eq. (2.1) with $\Delta t = 0.001$. The constant coefficient for the $1/k$ curve is 1.23.

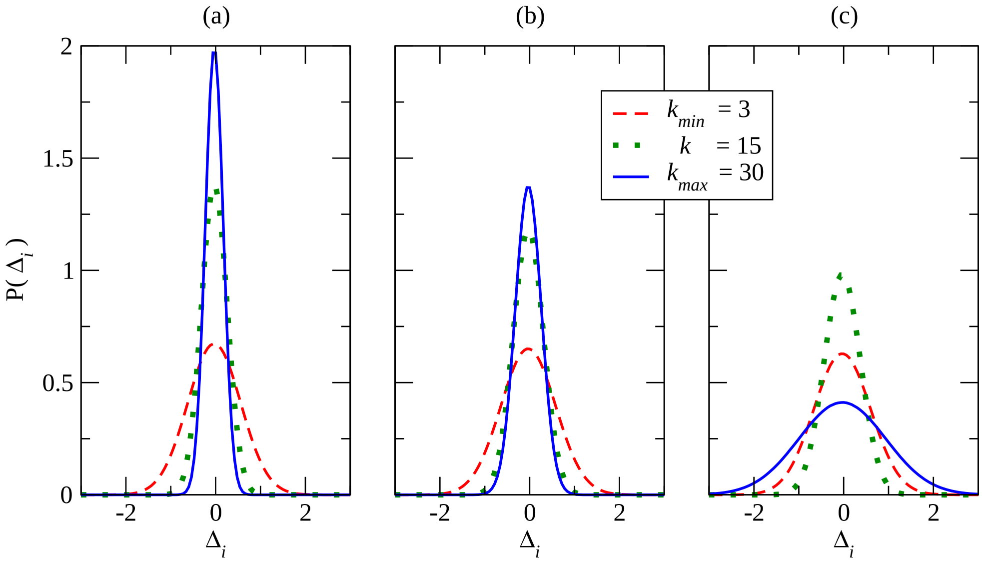

Figure 4.5: Probabilities for displacements from the mean Δ_i for three nodes that represent the lowest ($k_{\min}$), an intermediate, and the highest ($k_{\max}$) degree nodes for a typical $N = 100$ BA network. The three figures correspond to (a) 0%, (b) 50%, and (c) 95% of the critical delay $\tau_c = 0.05$

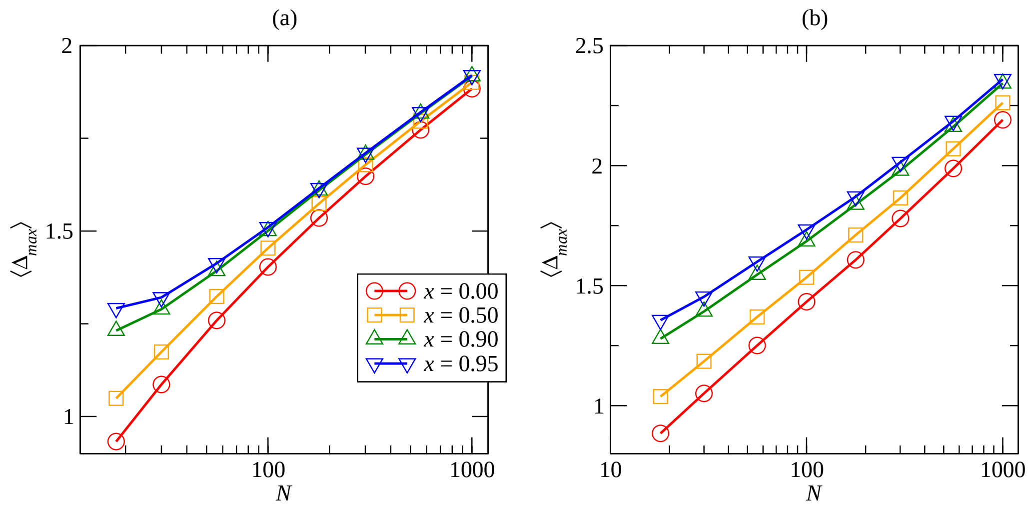

Figure 4.6: Average extreme fluctuations $\langle \Delta_{\max} \rangle$ for ensembles made up of 10^3 random networks for each size N. Each point is determined by numerically integrating Eq. (2.1) with $\Delta t = 0.001$ for networks that satisfy condition (2.23) from Chapter 2.

CHAPTER 5
Summary [4]

Through the investigations presented here, we have explored the impact and interplay of time delays, network structure, and coupling strength on synchronization and coordination in complex interconnected systems. The focus has only been on linear couplings, which already yields a rich phase diagrams and responses. While nonlinear effects are crucial in all real-life applications [7, 31, 32, 33], linearization and stability analysis about the synchronized state yields equations analogous to the ones considered here [8, 79]. Hence, the detailed analysis of the linear problems can provide some insights to the complex phase diagrams and response of nonlinear problems.

For a single uniform local delay, the synchronizability of a network is governed by a single eigenvalue (i.e., the largest) and the time delay. This result links the presence of larger hubs to the vulnerability of the system becoming unstable at smaller delays. The quality of system-wide synchronization within the stable regime is described by the width, which can be calculated exactly for arbitrary symmetric couplings, provided the spectrum is known. The boundaries of the region of synchronizability can also be expressed in terms of the delay and the overall coupling strength (associated with communication rate) to provide the general scaling behavior of the width inside this regime. These results underscore the importance of the interplay of stochastic effects, network connections, and time delays, in that how "less" (in terms of local communication efforts) can be "more" efficient (in terms of global performance).

For more general schemes with multiple time delays, stability analysis in general delay differential equations can be applied to ascertain the synchronizability of a network. For cases where – at least in principle – eigenmode decomposition is possible, the width obeys definite scaling behavior within the synchronizable regime.

[4] Portions of this chapter to appear in: D. Hunt, G. Korniss, B.K. Szymanski, "Network Synchronization and Coordination in a Noisy Environment with Time Delays", (in review).

However, in these cases it is not always the same eigenvalue that determines stability for all γ. This is in contrast to the special case $\gamma = 1$ when it is always the largest eigenvalue that determines synchronizability.

In the non-monotonic nature of the scaling function, there is a fundamental limit to how well a network can synchronize in the presence of noise. In the case when transmission and reaction are two independent and significant sources of delay, there is an additional parameter for tuning: the ratio of local delay to the total delay. By fixing the local delay and cutting across different values of the ratio, there is the possibility that the network will enter into and emerge from synchronizable regions. In such scenarios, increasing the transmission delay can be beneficial by returning the network to a synchronizable scheme.

Finally, we looked at the behavior of the extremes of the fluctuations in the presence of uniform time delay. The association of large hubs with the unsynchronizability of the network is reinforced by the observation that these hubs have the poorest response as the delay is increased. Of all the nodes, those with highest degree show the most deterioration in coordinating with the network. Ultimately, they are the nodes whose fluctuations diverge the fastest once the critical delay is reached. This shows that in order to extend the synchronizability of a network or to maintain a well-synchronized network for longer delays, avoiding large hubs can be very beneficial. Understanding all these influences can guide network design in order to maintain and optimize synchronization by balancing the trade-offs in internodal communication and local processing.

LITERATURE CITED

[1] M. Kalecki, “A Macrodynamic Theory of Business Cycles”, Econometrica **3**, 327 (1935).

[2] R. Frisch and H. Holme, “The Characteristic Solutions of a Mixed Difference and Differential Equation Occuring in Economic Dynamics”, Econometrica **3**, 225 (1935).

[3] U. Küchler, B. Mensch, “Langevin Stochastic Differential Equation Extended by a Time-Delayed Term”, Stoch. and Stoch. Rep. **40** 23 (1992).

[4] T. Ohira, T. Yamane, “Delayed stochastic systems”, Phys. Rev. E. **61** 1247 (2000).

[5] T. D. Frank, P. J. Beek, “Stationary solutions of linear stochastic delay-differential equations: Aplications to biological syatems”, Phys. Rev. E. **64** 021917 (2001).

[6] R. Olfati-Saber, J.A. Fax, and R.M. Murray, “Consensus and Cooperation in Networked Multi-Agent Systems”, Proc. IEEE **95**, 215 (2007).

[7] T. Hogg and B.A. Huberman, “Controlling Chaos in Distributed Systems”, IEEE Trans. on Sys., Man, and Cybernetics **21**, 1325 (1991).

[8] M.G. Earl and S.H. Strogatz, “Synchronization in oscillator networks with delayed coupling: A stability criterion”, Phys. Rev. E **67**, 036204 (2003).

[9] A. Arenas *et al.*, “Synchronization in complex networks”, Phys. Rep. **469**, 93 (2008).

[10] M. Barahona and L.M. Pecora, “Synchronization in Small-World Systems”, Phys. Rev. Lett. **89**, 054101 (2002).

[11] T. Nishikawa, *et al.*, “Heterogeneity in Oscillator Networks: Are Smaller Worlds Easier to Synchronize?”, Phys. Rev. Lett. **91**, 014101 (2003).

[12] C. E. La Rocca, L. A. Braunstein, and P. A. Macri, “Evolution equation for a model of surface relaxation in complex networks”, Phys. Rev. E **77**, 046120 (2008).

[13] C. E. La Rocca, L. A. Braunstein, and P. A. Macri, “Conservative model for synchronization problems in complex networks”, Phys. Rev. E **80**, 026111 (2009).

[14] C. Zhou, A.E. Motter, and J. Kurths, "Universality in the Synchronization of Weighted Random Networks", Phys. Rev. Lett. **96**, 034101 (2006).

[15] G. Korniss, "Synchronization in weighted uncorrelated complex networks in a noisy environment: Optimization and connections with transport efficiency", Phys. Rev. E **75**, 051121 (2007).

[16] G. Korniss, R. Huang, S. Sreenivasan, and B.K. Szymanski, "Optimizing Synchronization, Flow, and Robustness in Weighted Complex Networks", in *Handbook of Optimization in Complex Networks: Communication and Social Networks*, edited by M.T. Thai and P. Pardalos, Springer Optimization and Its Applications Vol. 58, (Springer, New York, 2012) pp. 61-96.

[17] T. Nishikawa and A.E. Motter, "Synchronization is optimal in nondiagonalizable networks", Phys. Rev. E **73**, 065106(R) (2006).

[18] T. Nishikawa and A.E. Motter, "Network synchronization landscape reveals compensatory structures, quantization, and the positive effect of negative interactions", Proc. Natl. Acad. Sci. U.S.A. **107**, 10342 (2010).

[19] A.-L. Barabási and R. Albert, "Emergence of Scaling in Random Networks", Science **286**, 509 (1999).

[20] R. Albert and A.-L. Barabási, "Statistical mechanics of complex networks", Rev. Mod. Phys. **74**, 47 (2002).

[21] P. Erdös, A. Rényi, "On the evolution of random graphs", Publ. Math. Inst. Hung. Acad. Sci, Vol. 5, pp. 17-61 (1960)

[22] R. Sipahi *et al*, "Stability and Stabilization of Systems with Time Delay", IEEE Contr. Sys. **31**, 38 (2011)

[23] G.E. Hutchinson, "Circular Causal Systems in Ecology", Ann. N.Y. Acad. Sci. **50**, 221 (1948).

[24] R.M. May, "Time-Delay Versus Stability in Population Models with Two and Three Trophic Levels", Ecology **54**, 315–325 (1973).

[25] H. M. Smith, "Synchronous Flashing of Fireflies", Science **82**, 151 (1935).

[26] C. G. Reynolds "Flocks, Herds, and Schools: A Distributed Behavioral Model", *Computer Graphics* 21(4) pp. 25-34 (1987).

[27] F. Cucker and S. Smale, "Emergent Behavior in Flocks", IEEE Trans. Automat. Contr. **52**, 852 (2007).

[28] T. Vicsek *et al.*, "Novel Type of Phase Transition in a System of Self-Driven Particles", Phys. Rev. Lett. **75**, 1226 (1995).

[29] S. Saavedra, K. Hagerty, and B. Uzzi, "Synchronicity, Instant Messaging and Performance among Financial Traders", Proc. Natl. Acad. Sci. U.S.A. **108**, 5296 (2011).

[30] E. Izhikevich, "Synchronization of elliptic bursters", SIAM Rev. **43**, 315 (2001).

[31] Q. Wang, Z. Duan, M. Perc, and G. Chen, "Synchronization transitions on small-world neuronal networks: Effects of information transmission delay and rewiring probability", Europhys. Lett. **83**, 50008 (2008).

[32] Q. Wang, M. Perc, Z. Duan, and G. Chen, "Synchronization transitions on a scale-free neuronal networks due to finite information transmission delays", Phys. Rev. E **80**, 026206 (2009).

[33] Q. Wang, G. Chen, M. Perc, "Synchronous bursts on scale-free neuronal networks with attractive and repulsive coupling", PLoS One **6** e15851 (2011).

[34] J.G. Milton, J.L. Cabrera, and T. Ohira, "Unstable dynamical systems: Delays, noise and control", Europhys. Lett. **83**, 48001 (2008).

[35] J. Milton, J.L. Townsend, M.A. King, T. Ohira, "Balancing with positive feedback: the case for discontinuous control", Phil. Trans. R. Soc. A **367**, 1181 (2009).

[36] J.L. Cabrera and J.G. Milton, "On-off intermittency in a human balancing task", Phys. Rev. Lett. **89**, 157802 (2002).

[37] J.L. Cabrera, C. Luciani, and J. Milton, "Neural control on multiple time scales: Insights form human stick balancing", Cond. Matt. Phys. **9**, 373 (2006).

[38] R. Johari and D. Kim Hong Tan, "End-to-End Congestion Control for the Internet: Delays and Stability", IEEE/ACM Trans. Networking **9**, 818 (2001).

[39] R. Olfati-Saber and R.M. Murray, "Consensus Problems in Networks of Agents with Switching Topology and Time-Delays", IEEE Trans. Automat. Contr. **49**, 1520 (2004).

[40] T.J. Ott, "On the Ornstein-Uhlenbeck Process with Delayed Feedback", http://www.teunisott.com/Papers/TCP_Paradigm/Del_O_U.pdf (2006).

[41] G. Korniss, M.A. Novotny, H. Guclu, and Z. Toroczkai, P.A. Rikvold, "Suppressing Roughness of Virtual Times in Parallel Discrete-Event Simulations", Science **299**, 677 (2003).

[42] G. Korniss, Z. Toroczkai, M.A. Novotny, and P.A. Rikvold, "From Massively Parallel Algorithms and Fluctuating Time Horizons to Non-equilibrium Surface Growth", Phys. Rev. Lett. **84** 1351 (2000).

[43] H. Guclu, *et al.* "Synchronization Landscapes in Small-World-Connected Computer Networks", Phys. Rev. E **73** 066115 (2006).

[44] H. Guclu, G. Korniss, and Z. Toroczkai, "Extreme fluctuations in noisy task-completion landscapes on scale-free networks", Chaos **17** 026104 (2007).

[45] G. Orosz and G. Stepan, "Subcritical Hopf bifurcations in a car-following model with reaction-time delay", Proc. R. Soc. A **462** 2643 (2006)

[46] G. Orosz, R.E. Wilson and G. Stepan, "Traffic jams: dynamics and control", Phil. Trans. R. Soc. A **368**, 4455 (2010)

[47] J.A. Fax and R.M. Murray, "Information Flow and Cooperative Control of Vehicle Formations", IEEE Trans. Automat. Contr. **49**, 1465 (2004).

[48] H. Hong, M. Y. Choi, B. J. Kim, "Synchronization on small-world networks" Phys. Rev. E **65** 026139 (2002).

[49] Y. Kuramoto, in *Proceedings of the International Symposium on Mathematical Problems in Theoretical Physics*, edited by H. Araki, Lecture Notes in Physics Vol. 30 (Springer, New York, 1975) p. 420.

[50] G. Michael, Z. Jabeen, B. Chakraborty, "Phase and frequency entrainment in locally coupled phase oscillators with repulsive interactions", Phys. Rev. E **83** 046206 (2011).

[51] G. Heinrich *et al.*, "Collective dynamics in optomechanical arrays", Phys. Rev. Lett **107** 043603 (2011).

[52] S.F. Edwards and D.R. Wilkinson, "The surface statistics of a granular aggregate", Proc. R. Soc. London, Ser A **381**, 17 (1982).

[53] C.W. Gardiner, *Handbook of Stochastic Methods* 2nd ed. (Springer-Verlag, New York, 1985).

[54] N. Goldenfeld, *Lectures on Phase Transitions and the Renormalization Group* (Addison-Wesley, New York, 1992).

[55] D.J. Watts and S.H. Strogatz, "Collective dynamics of 'small-world' networks", Nature **393**, 440 (1998).

[56] S.N. Dorogovtsev and J.F.F. Mendes, "Evolution of networks", Adv. in Phys. **51**, 1079 (2002).

[57] R. Monasson, "Diffusion, localization and dispersion relations on 'small-world' lattices", Eur. Phys. J. B **12**, 555 (1999).

[58] B. Kozma and G. Korniss, “Stochastic Growth in a Small World”, in *Computer Simulation Studies in Condensed Matter Physics XVI*, edited by D.P. Landau, S.P. Lewis, and H.-B. Schttler, Springer Proceedings in Physics Vol. 95 (Springer-Verlag, Berlin, 2004) pp. 29-33.

[59] B. Kozma, M. B. Hastings, and G. Korniss, “Roughness Scaling for Edwards-Wilkinson Relaxation in Small-World Networks”, Phys. Rev. Lett. **92**, 108701 (2004).

[60] D.-H. Kim and A.E. Motter, “Ensemble Averageability in Network Spectra”, Phys. Rev. Lett. **98**, 248701 (2007).

[61] D. Hunt, G. Korniss, B.K. Szymanski, “Network Synchronization in a Noisy Environment with Time Delays: Fundamental Limits and Trade-Offs”, Phys. Rev. Lett. **105**, 068701 (2010).

[62] D. Hunt, G. Korniss, B.K. Szymanski, “Network Synchronization and Coordination in a Noisy Environment with Time Delays”, (in review).

[63] M. Bambi, “Endogenous growth and time-to-build: The AK case”, J. Econ. Dynamics and Control **32**, 1015 (2008).

[64] S. Ruan, “Delay Differential Equations in Single Species Dynamics”, in *Delay Differential Equations and Applications*, edited by O. Arino, M.L. Hbid, and E.A. Dads, NATO Science Series II: Mathematics, Physics and Chemistry, Vol. 205 (Springer, Berlin, 2006) pp. 477–517.

[65] A. Amann, E. Scholl, and W. Just, “Some basic remarks on eigenmode expansions of time-delay dynamics”, Physica A **373**, 191 (2007).

[66] D. Hunt, G. Korniss, B.K. Szymanski, “The impact of competing time delays in coupled stochastic systems”, Phys. Lett. A **375**, 880 (2011).

[67] S. Hod, “Analytic Treatment of the Network Synchronization Problem with Time Delays”, Phys. Rev. Lett. **105**, 208701 (2010).

[68] N.D. Hayes, “Roots of the Transcendental Equation Associated with a Certain Difference-Differential Equation”, J. London Math. Soc. **s1-25**, 226 (1950).

[69] N.G. van Kampen, “Ito versus Stratonovich”, J. Stat. Phys. **24**, 175 (1981).

[70] M. Fiedler, “Algebraic connectivity of graphs”, Czech. Math. J. **23**, 298 (1973).

[71] W.N. Anderson and T.D. Morley, “Eigenvalues of the Laplacian of a graph”, Lin. Multilin. Algebra **18**, 141 (1985).

[72] M. Boguña, and R. Pastor- Satorras, and A. Vespignani, “Cut-offs and finite-size effects in scale-free networks”, Eur. Phys. J. B **38**, 205 (2004).

[73] M. Catanzaro, M. Boguña, and R. Pastor-Satorras, “Generation of uncorrelated random scale-free networks”, Phys. Rev. E **71**, 027103 (2005).

[74] A. E. Motter, “Bounding network spectra for network design”, New J. Phys. **9** 182 (2007).

[75] S.G. Krantz, *Handbook of Complex Variables* (Birkhauser, Boston, MA, 1999).

[76] J.M. Höfener, G.C. Sethia, T. Gross, “Stability and Resonance in Networks of Delay-Coupled Delay Oscillators”, Europhys. Lett. **95**, 40002 (2011).

[77] T. Luzyanina and D. Roose, “Numerical stability analysis and computation of Hopf bifurcation points for delay differential equations”, J. Comp. Appl. Math. **72** 379 (1996).

[78] F.M. Atay, Phys. Rev. Lett. **91**, 094101 (2003).

[79] A. Papachristodoulou, A. Jadbabaie, and U. Münz, “Effects of Delay in Multi-Agent Consensus and Oscillator Synchronization”, IEEE Trans. Automat. Contr. **55** , 1471 (2010).

[80] S. Raychaudhuri, M. Cranson, C. Przybyla, and Y. Shapir “Maximal Height Scaling of Kinetically Growing Surfaces”, Phys. Rev. Lett. **87**, 136101 (2001).

[81] H. Guclu and G. Korniss, “Extreme Fluctuations in Small-World-Coupled Autonomous Systems with Relaxational Dynamics”, Fluct. and Noise Lett. **5**, L43 (2005).

[82] H. Guclu and G. Korniss, “Extreme Fluctuations in Small-Worlds with Relaxational Dynamics” Phys. Rev. E **69** 065104(R) (2004).

[83] R. A. Fisher and L. H. C. Tippett, “The frequency distribution of the largest or smallest member of a sample”, Proc. Camb. Philos. Soc. **24**, 180191 (1928).

[84] E. J. Gumbel, *Statistics of Extremes*, (New York, Columbia University Press, 1958)

[85] *Extreme Value Theory and Applications*, eds. J. Galambos, J. Lechner and E. Simin, (Kluwer Academic Publishers, Dordrecht 1994)